THEORY OF TWO-POINT CORRELATIONS OF JET NOISE

Herbert S. Ribner

Langley Research Center
Hampton, Va. 23665

NATIONAL AERONAUTICS AND SPACE ADMINISTRATION • WASHINGTON, D. C. • DECEMBER 1976

completed 26 May 77 SM

ERRATA

NASA Technical Note D-8330

THEORY OF TWO-POINT CORRELATIONS OF JET NOISE

Herbert S. Ribner
December 1976

Page 12, equation (15): Replace $\overline{\left(u_x^a\right)^2\left(u_x^b\right)^2}$ with $\overline{\left(u_x^a\right)^2}\ \overline{\left(u_x^b\right)^2}$

Page 14, equation (22): Replace $d^3\vec{\eta}$ with $d^3\vec{\eta}\ d^3\vec{Y}$.

Page 20, equation (38): The first line of the right side of the equation should read

$$\frac{n_1^a n_1^b n_i^a n_j^b \rho_o^2}{4\pi^2 c_o^4 x^2}\iint \omega_f^4 e^{-\omega_f|\Delta|} U^2\left(\vec{Y}\right)\overline{u_1^2}\left(\vec{Y}\right)$$

Page 20, line preceding equation (40): Replace $U^2\left(\vec{Y}\right)$ with $\overline{u_1^2}\left(\vec{Y}\right)$.

Page 21, equation (42): Replace the factor $g_2 g_3$ with the factor $\rho_o^2 g_2 g_3$.

Page 22, equation (43): Replace the factor $\frac{g_1 g_2}{2^{1/2}\pi}$ with the factor $\frac{\rho_o^2 g_1 g_2}{2^{1/2}\pi}$.

Page 22, equation (44): Replace the factor $\frac{g_2 g_3}{4\pi}$ with the factor $\frac{\rho_o^2 g_2 g_3}{4\pi}$.

Page 26, line 3: Replace the word "larger" with the word "smaller" so that the sentence reads

This yields manyfold smaller values of f_f.

Page 27, line 12: Replace equations (16) with equation (32).

Page 29, line 10: Replace figures 7 and 10 with figure 7 and other figures.

Page 30: Move (and amplitude) on line 3 from bottom of page to end of sentence so that the sentence reads

The sound emission from each small volume is seen to consist of a rather directional quadrupole pattern whose lobes fluctuate randomly in direction (and amplitude).

ISSUED MAY 1977

1. Report No.	2. Government Accession No.	3. Recipient's Catalog No.
NASA TN D-8330		

4. Title and Subtitle
THEORY OF TWO-POINT CORRELATIONS OF JET NOISE

5. Report Date
December 1976

6. Performing Organization Code

7. Author(s)
Herbert S. Ribner

8. Performing Organization Report No.
L-11058

9. Performing Organization Name and Address
NASA Langley Research Center
Hampton, VA 23665

10. Work Unit No.
505-03-11-02

11. Contract or Grant No.

12. Sponsoring Agency Name and Address
National Aeronautics and Space Administration
Washington, DC 20546

13. Type of Report and Period Covered
Technical Note

14. Sponsoring Agency Code

15. Supplementary Notes
Herbert S. Ribner: Staff Scientist, now back at University of Toronto, Institute for Aerospace Studies.

16. Abstract

A large body of careful experimental measurements of two-point correlations of far-field jet noise has been carried out and was briefly reported recently by Lucio Maestrello in NASA TM X-72835. The results were not altogether as expected and motivated the present effort to bring theory to bear. The model of jet-noise generation is an approximate version of an earlier work of Ribner, based on the foundations of Lighthill. The model incorporates isotropic turbulence superimposed on a specified mean shear flow, with assumed space-time velocity correlations, but with source convection neglected. The particular vehicle is the Proudman format, and the previous work (mean-square pressure) is extended to display the two-point space-time correlations of pressure.

The shape of polar plots of correlation is found to derive from two main factors: (1) the noncompactness of the source region, which allows differences in travel times to the two microphones – the dominant effect – and (2) the directivities of the constituent quadrupoles – a weak effect. The noncompactness effect causes the directional lobes in a polar plot to have pointed tips (cusps) and to be especially narrow in the plane of the jet axis. In these respects, and in the quantitative shapes of the normalized correlation curves, results of the theory show generally good agreement with Maestrello's experimental measurements.

17. Key Words (Suggested by Author(s))	18. Distribution Statement
Jet noise Acoustics Aeroacoustics Correlations	Unclassified – Unlimited Subject Category 71

19. Security Classif. (of this report)	20. Security Classif. (of this page)	21. No. of Pages	22. Price*
Unclassified	Unclassified	58	$4.25

*For sale by the National Technical Information Service, Springfield, Virginia 22161

CONTENTS

SUMMARY 1

INTRODUCTION 1

SYMBOLS 3

OVERVIEW OF THEORY 7

ANALYTICAL DEVELOPMENT 8

- Governing Equations 8
- Self-Noise 12
- Integral Over Noncompact Jet 16
- Shear Noise 19
- Summarized Predictions 22

DISCUSSION 24

- Comparison With Experiments of Maestrello 24
- Further Considerations 28

CONCLUSIONS 30

APPENDIX A – QUADRUPOLES WITH FLUCTUATING ORIENTATION: THE BEAM PATTERN CONCEPT 32

APPENDIX B – EVALUATION OF NONCOMPACTNESS FACTORS FOR CASE I: $\theta_a = \theta_b = \theta$, $\varphi_a = 0$ 35

APPENDIX C – EVALUATION OF NONCOMPACTNESS FACTORS FOR CASE II: $\varphi_b = \varphi_a$ 37

APPENDIX D – REDUCTION OF THE SHEAR-NOISE INTEGRAL, EQUATION (42) 39

REFERENCES 41

FIGURES 43

THEORY OF TWO-POINT CORRELATIONS OF JET NOISE

Herbert S. Ribner*
Langley Research Center

SUMMARY

A large body of careful experimental measurements of two-point correlations of far-field jet noise has been carried out and was briefly reported recently by Lucio Maestrello in NASA TM X-72835. The results were not altogether as expected and motivated the present effort to bring theory to bear. The model of jet-noise generation is an approximate version of an earlier work of Ribner, based on the foundations of Lighthill. The model incorporates isotropic turbulence superimposed on a specified mean shear flow, with assumed space-time velocity correlations, but with source convection neglected. The particular vehicle is the Proudman format, and the previous work (mean-square pressure) is extended to display the two-point space-time correlations of pressure.

The shape of polar plots of correlation is found to derive from two main factors: (1) the noncompactness of the source region, which allows differences in travel times to the two microphones – the dominant effect – and (2) the directivities of the constituent quadrupoles – a weak effect. The noncompactness effect causes the directional lobes in a polar plot to have pointed tips (cusps) and to be especially narrow in the plane of the jet axis. In these respects, and in the quantitative shapes of the normalized correlation curves, results of the theory show generally good agreement with Maestrello's experimental measurements.

INTRODUCTION

A quarter of a century of jet-noise research has focused almost exclusively on the response of a single microphone. Until now there have been no studies of the joint response of two microphones in the far field, that is, of two-point correlations of sound pressure. This is understandable because the difficulty of theoretical prediction has been so formidable that one leans toward the simpler case.

Recently, however, rather different theories (e.g., those of Mani (refs. 1 and 2) and Ribner (refs. 3 and 4)) have demonstrated considerable success in predicting

*Staff Scientist, now back at University of Toronto, Institute for Aerospace Studies.

single-microphone directional response (refs. 2, 5, and 6). This points up a certain insensitivity of the single-microphone response (mean-square pressure) to details of the theoretical model. The two-microphone correlations, which provide much more information, would be expected to be less ambiguous in their dependence on details of the model. Such cross-correlations could conceivably provide a sensitive test of validity.

With this motivation, a large body of careful experimental measurements of two-point jet-noise correlations has been carried out by Maestrello and is reported in a recent paper (ref. 7) along with theoretical considerations. The results were not altogether as expected and, in accord with the above notions, motivated the present attempt at a theoretical explanation.

The model of jet-noise generation is an approximate form of that of Ribner (refs. 3 and 4), which is a development of the Lighthill (refs. 8 and 9) formalism. It postulates isotropic turbulence superimposed on a specified mean shear flow. The Proudman (ref. 10) formalism is used, wherein the momentum flux in the direction of the observer governs the combined emission of the Lighthill quadrupoles in that direction. The space-time velocity correlations associated with this momentum flux are described by a simple mathematical model. The development of reference 4 (mean-square pressure) is extended to provide the two-point correlations of pressure. A series of simplifying assumptions and restrictions, based on physical considerations, is applied to render the sixfold integration tractable.

An important restriction is the complete omission of all source convection and refraction effects. The convection effects are expected to be predominantly amplitude changes at points of the sound field, with much less change in the pattern coherence between two points. Hence, normalizing the two-point pressure correlation by the product of the rms pressures at the two points should largely cancel the contribution of convection. The refraction effects can be anticipated with less assurance; nevertheless, the normalization should partially offset them.

The single-microphone case likewise calls for a sixfold integration. However, the major features of the directivity can be inferred after only a threefold integration. This yields the sound emission from a unit volume of a jet whose directional properties are fairly representative of those of the entire jet in a given narrow frequency band. That is not so, however, for the two-microphone correlation; hence the much more demanding sixfold integration is required.

The details of the derivation of the two-point pressure correlations are developed in the body of the paper and in appendixes A to D. The results are relatively simple closed-form expressions. The theoretical predictions are compared with the measured data of Maestrello (ref. 7) for a number of cases.

SYMBOLS

$C_{ij}(\vec{\eta})$	space factor in correlation $\overline{u_i^a u_j^b}$, specified in equations (21)
c_o	ambient speed of sound
D	jet diameter
$F\left(\frac{r-R}{Y_1}\right)$	function defined in equation (27)
f_f	frequency characterizing the local turbulence, treated as a "typical" frequency
$f(\eta)$	$= e^{-\pi^2\eta^2/L^2}$
$g(\tau_1)$	time delay factor in correlation $\overline{u_i^a u_j^b}$, specified as $e^{-\omega_f\lvert\tau_1\rvert}$
g_1, g_2, g_3	constants
I,J	noncompactness integrals appearing in equations (46) and appendix B
L	effective scale of turbulence
ℓ	effective length of source region
M_j	jet Mach number, U_j/c_o
N_{Str}	Strouhal number, $f_f D/U_j$
$\vec{n}$	unit vector along $\vec{x}$
n_i	ith component of $\vec{n}$ in basic reference frame (fig. 1)
$\hat{n}_i$	ith component of $\vec{n}$ in special reference frame (eqs. (17))
P	pressure
p	far-field pressure perturbation; also point of pressure measurement

q_{se} $= 4\langle\omega_f\rangle\left(R/c_o\right)\left|\sin\theta_b \sin\left(\varphi_b/2\right)\right|$

q_{sh} $= 2\langle\omega_f\rangle\left(R/c_o\right)\left|\sin\theta_b \sin\left(\varphi_b/2\right)\right|$

R radius of jet; also correlation function

r radial distance from jet axis

T_{ij} $= \rho_o v_i v_j + \tau_{ij} + \left(P - c_o{}^2\rho\right)\delta_{ij}$

t time of signal reception

$\hat{t}$ time of signal emission

$\vec{U}$ local mean flow velocity

U_j jet nozzle velocity

U_x component of $\vec{U}$ along $\vec{x}$

$\vec{u}$ local turbulence velocity

u_i component of $\vec{u}$

u_x component of $\vec{u}$ along $\vec{x}$

$\vec{v}$ local resultant velocity, $\vec{u} + \vec{U}$

v_i component of $\vec{v}$

v_x component of $\vec{v}$ along $\vec{x}$

$\vec{x}$ position vector of field point

x_i component of $\vec{x}$

$\vec{Y}$ position vector of centroid of correlation volume, or "eddy"

Y_i component of $\vec{\vec{Y}}$

$\vec{y}$ position vector of source point

β $= \dfrac{2 \times \text{Maximum shear-noise intensity}}{\text{Self-noise intensity}}$ (see eq. (45))

γ azimuth angle in cylindrical polar coordinates

Δ time delay between emissions for simultaneous reception at p_a and p_b

δ $= \dfrac{\ell \langle \omega_f \rangle}{c_o} \left| \cos \theta_b - \cos \theta_a \right|$

δ_{ij} Kronecker delta, $\delta_{ij} = \begin{cases} 1 & (i = j) \\ 0 & (i \neq j) \end{cases}$

ϵ dummy variable

$\vec{\eta}$ separation of source points, $\vec{y}^a - \vec{y}^b$

η_i component of $\vec{\eta}$

θ polar angle, $x_1 = x \cos \theta$

λ wavelength

μ azimuth angle in special reference frame (see sketch (a) following eqs. (17))

ρ density

ρ_o ambient density

σ constant (eq. (35))

τ time delay between signal receptions at $\vec{\vec{x}}^a$ and $\vec{\vec{x}}^b$ (specified)

τ_1 time delay between signal emissions, $\tau + \Delta$

τ_{ij} viscous compressive stress tensor

φ azimuth angle, $x_2 = x \cos\theta \cos\varphi$

ψ angle between $\vec{x}^a$ and $\vec{x}^b$ $\left(\text{Case I: } \cos\psi = \cos^2\theta + \sin^2\theta \cos\varphi_b;\right.$
$\left.\text{Case II: } \psi = \left|\theta_b - \theta_a\right|\right)$

ω radian frequency, $2\pi f$

ω_f $= 2\pi f_f$

Subscripts or superscripts:

a associated with sound emission to point $\vec{x}^a$

b associated with sound emission to point $\vec{x}^b$

Subscripts:

i ith vector component (e.g., $i = 1$ denotes component along x_1)

i,j tensor indices

n radial direction (normal to shear layer)

se self-noise

sh shear noise

Brackets:

$[\,]$ evaluated at retarded time

$\langle\,\rangle$ average over mixing region

A bar over a quantity denotes a time average.

OVERVIEW OF THEORY

The analytical development in the following sections is long and involved. Thus it seems worthwhile to present a simplified overview at this point with the aid of a series of figures. Figure 1 shows multiplication and time averaging of the governing equations for sound pressures p_a and p_b to yield the $\overline{p_a p_b}$ correlation in schematic form (cf. refs. 3 and 4): the self-noise and shear-noise components of the source term (integrand) are singled out. Figure 2 brings out the principal new feature that arises when one microphone is replaced by two: the travel times from a source point to the two microphones are different in general. If the source region is noncompact (dimensions greater than a typical wavelength of the sound field), the difference in travel times will substantially reduce the $\overline{p_a p_b}$ correlation.

Figure 3 exhibits the phenomena in a more physical fashion. It shows how the source-observer difference in travel times τ (which must be averaged over all source positions) gives rise to a cusp[1] in the correlation pattern as $\psi \to 0$. The main point is that microphone b records somewhat the same pressure-time signature as microphone a, but with the signature delayed by an amount τ that depends on the geometry. The cross-correlation $\overline{p_a p_b}$ expressed as a function of time delay τ is thus essentially the auto-correlation $\overline{p_a p_a'}(\tau)$. Expressing τ as a function of ψ (and of $\theta_a, \varphi_a, \theta_b, \varphi_b$ as parameters) in effect maps $\overline{p_a p_a'}(\tau)$ into $\overline{p_a p_b}(\psi, \theta_a, \text{etc.})$. In this mapping the cusp, which is characteristic of measured autocorrelations, reappears in the cross-correlation.

The pressure signatures at microphones a and b due to a source element, although generally similar, differ by more than just the time shift τ: they reflect the composite nature of the sources (fig. 4). The source strength density at a point consists of a superposition of six kinds of quadrupole T_{ij} – three lateral and three longitudinal – some of whose directional patterns are shown in figure 4. At a given instant their relative amplitudes appear to be random; they are, however, related statistically, and the two-microphone correlation $\overline{p_a p_b}$ involves a statistical average.

The nature of the sources dictates the basic correlation that remains when the noncompactness effects are omitted: an example is the hourglass shape shown in figure 4. The basic correlation must be multiplied by the noncompactness factor to give the overall correlation. In the example case the forward lobe ($\psi < 180^\circ$) will be large; the rearward lobe ($\psi > 180^\circ$), very small. This will be alluded to in the Discussion, in the comparison of theory and experiment.

[1]The term cusp as used herein indicates a symmetric discontinuous finite slope of $\overline{p_a p_b}(\psi)$ at $\psi = 0$, rather than a discontinuous infinite slope.

It may be of interest to return to the random (in time) distribution of six quadrupole directional patterns. In the present model these reduce to three (T_{11}, T_{12}, T_{13}) for the shear-noise contribution. Appendix A shows that T_{12} and T_{13} jointly produce a sound pattern of fixed shape (but fluctuating amplitude) whose directional lobes fluctuate stochastically in orientation about the jet axis. This is a variation of the "beam pattern" concept put forward by Maestrello and Pao (ref. 11), elaborated and refined in reference 12, and supported by experiment (ref. 13). The fluctuating beam pattern sweeps randomly over the two separated microphones a and b, and the time average of the contribution to $\overline{p_a p_b}$ is governed solely by the pattern shape and microphone positions.

To round out the picture for the shear noise, refer now to the T_{11} quadrupole: its beam pattern is of the form $A(t)\cos^2\theta$. This figure-eight beam pattern fluctuates solely in amplitude while maintaining a fixed direction alined with the jet axis.

ANALYTICAL DEVELOPMENT

Governing Equations

Lighthill (refs. 8 and 9) has shown that the sound pressure radiated to a point $\vec{x}$ in the far field by a localized unsteady or turbulent flow is given by

$$p(\vec{x},t) = \left(4\pi c_o^2\right)^{-1} \frac{x_i x_j}{x^3} \int \left[\frac{\partial^2 T_{ij}}{\partial t^2}\right] d^3\vec{y} \tag{1}$$

where T_{ij} is a quadrupole strength density,

$$T_{ij} = \rho v_i v_j + \tau_{ij} + \left(P - c_o^2 \rho\right) \delta_{ij} \tag{2}$$

that is normally dominated by the unsteady momentum flux $\rho v_i v_j$, for example, in a turbulent jet at ambient temperature. Here τ_{ij} is the viscous compressive stress tensor; P, the local pressure; ρ, the density; c_o, the ambient speed of sound; v_i, the velocity; and $\delta_{ij} = 0$ or 1, as $i \neq j$ or $i = j$. The brackets designate retarded time (to be specified later); $i, j = 1, 2$, or 3; and repeated indices are summed over. The flow occupies only a limited region around the origin of coordinates.

The quadrupole strength density T_{ij} is approximated as $\rho_o v_i v_j$ and, following Proudman (ref. 10), $x_i v_i / x$ is observed to be the component v_x of the resultant velocity along $\vec{x}$. For two points $\vec{x}^a$ (at time t_a) and $\vec{x}^b$ (at time t_b) – with $|\vec{x}^a| = |\vec{x}^b| = x$ – this yields

$$\left.\begin{aligned} p_a(\vec{x}^a,t) &= \left(4\pi c_o{}^2 x\right)^{-1} \rho_o \int \left[\frac{\partial^2 \left(v_x^a\right)^2}{\partial t^2}\right] d^3\vec{y}^a \\ p_b(\vec{x}^b,t) &= \left(4\pi c_o{}^2 x\right)^{-1} \rho_o \int \left[\frac{\partial^2 \left(v_x^b\right)^2}{\partial t^2}\right] d^3\vec{y}^b \end{aligned}\right\} \tag{3}$$

where the brackets signify evaluation at the respective retarded times

$$\left.\begin{aligned} \hat{t}_a &= t_a - \frac{\left|\vec{x}^a - \vec{y}^a\right|}{c_o} \\ \hat{t}_b &= t_b - \frac{\left|\vec{x}^b - \vec{y}^b\right|}{c_o} \end{aligned}\right\} \tag{4}$$

Since $\vec{x}$ and $\vec{x} - \vec{y}$ are nearly parallel for $\vec{x}$ in the acoustic far field, where $x \gg y$, these are approximately (fig. 5)

$$\left.\begin{aligned} \hat{t}_a &= t_a - \frac{x}{c_o} + \frac{\vec{y}^a \cdot \vec{n}^a}{c_o} \qquad \left(\vec{n}^a \equiv \vec{x}^a/x\right) \\ \hat{t}_b &= t_b - \frac{x}{c_o} + \frac{\vec{y}^b \cdot \vec{n}^b}{c_o} \qquad \left(\vec{n}^b \equiv \vec{x}^b/x\right) \end{aligned}\right\} \tag{5}$$

Thus, the correlation of sound pressure at <u>equidistant</u> points $\vec{x}^a$ and $\vec{x}^b$, at respective times $t_a = t$ and $t_b = t - \tau$, is

$$R\left(\vec{x}^a,\vec{x}^b,\tau\right) \equiv \overline{p\left(\vec{x}^a,t\right)p\left(\vec{x}^b,t-\tau\right)}$$

$$= \frac{\rho_o{}^2}{16\pi^2 c_o{}^4 x^2} \iint \overline{\left[\frac{\partial^2}{\partial t^2}\left(v_x^a\right)^2\right]_{\hat{t}_a} \left[\frac{\partial^2}{\partial t^2}\left(v_x^b\right)^2\right]_{\hat{t}_b}}\, d^3\vec{y}^a d^3\vec{y}^b \tag{6}$$

The directions of the vectors $\vec{x}^a$ and $\vec{x}^b$ to the two observer points have been designated by unit vectors $\vec{n}^a$ and $\vec{n}^b$. The separation between the two source points $\vec{y}^a$

and $\vec{y}^b$ may be designated $\vec{\eta}$ and the midpoint by $\vec{Y}$. The relations are

$$\vec{\eta} = \vec{y}^a - \vec{y}^b \qquad \vec{Y} = \frac{1}{2}\left(\vec{y}^a + \vec{y}^b\right) \tag{7}$$

The difference in travel times from the sources at $\vec{y}^a, \vec{y}^b$ to the respective observers at $\vec{x}^a, \vec{x}^b$ is, according to equations (5),

$$\Delta = \frac{\vec{y}^a \cdot \vec{n}^a}{c_o} - \frac{\vec{y}^b \cdot \vec{n}^b}{c_o}$$

$$= \frac{\vec{Y} \cdot \left(\vec{n}^a - \vec{n}^b\right)}{c_o} + \frac{\vec{\eta} \cdot \left(\vec{n}^a + \vec{n}^b\right)}{2c_o} \tag{8}$$

If the time delay between receptions of the two signals at $\vec{x}^a$ and $\vec{x}^b$ is

$$t_a - t_b = \tau \quad \text{(specified)} \tag{9}$$

then the time delay between emissions from $\vec{y}^a$ and $\vec{y}^b$ is

$$\hat{t}_a - \hat{t}_b \; (\equiv \tau) = \tau + \Delta \tag{10}$$

Equation (6) may be transformed into

$$R\left(\vec{x}^a, \vec{x}^b, \tau\right) = \rho_o{}^2 \left(16\pi^2 c_o{}^4 x^2\right)^{-1} \iint \left[\frac{\partial^4}{\partial \tau^4} \overline{\left(v_x^a\right)^2 \left(v_x^b\right)^2}\right] d^3\vec{\eta}\, d^3\vec{Y} \tag{11}$$

where $\left(v_x^a\right)^2$ is evaluated at $\vec{y}^a, \hat{t}_a$ and $\left(v_x^b\right)^2$ at $\vec{y}^b, \hat{t}_b$. The flow is postulated in the statistical sense as stationary and locally homogeneous; thus the correlation $\overline{\left(v_x^a\right)^2 \left(v_x^b\right)^2}$ depends primarily on the time delay τ_1 and the separation $\vec{\eta}$. The brackets imply evaluation at a time delay $\tau_1 = \tau + \Delta$. In this work the reference frame is stationary and the sources are stationary as well: they are specified as being unconvected by the mean flow.

In what follows, a model for the two-point space-time velocity correlation $\overline{\left(v_x^a\right)^2 \left(v_x^b\right)^2}$ is postulated. The model is limited to the jet mixing region and varies with position $\vec{Y}$ in a fashion dictated by similarity concepts. A series of simplifying

assumptions, based on physical considerations, is applied to render the sixfold integration tractable. With this same motivation the final analysis is restricted to zero time delay τ between reception of signals at p_a and p_b. (This restriction may be relaxed without difficulty.) The final two-point sound pressure correlation thus reflects a number of approximations in the model.

The instantaneous local velocity $\vec{v}$ is the resultant of the turbulence and stream velocities:

$$\vec{v} = \vec{u} + \vec{U} \tag{12}$$

with $\vec{U}$ taken parallel to the jet axis and $\vec{u}$ having zero mean. Since v_x is the component of $\vec{v}$ along $\vec{x}$, then

$$v_x^2 = u_x^2 + 2U_x u_x + U_x^2 \tag{13}$$

$$\begin{aligned}\overline{\left(v_x^a\right)^2\left(v_x^b\right)^2} = {} & \overline{\left(u_x^a\right)^2\left(u_x^b\right)^2} + 4U_x^a U_x^b \overline{u_x^a u_x^b} + \left(U_x^a\right)^2\left(U_x^b\right)^2 \\ & + \left(U_x^a\right)^2\overline{\left(u_x^b\right)^2} + \left(U_x^b\right)^2\overline{\left(u_x^a\right)^2} + 2U_x^a\left(U_x^b\right)^2 \overline{u_x^a} \\ & + 2U_x^b\left(U_x^a\right)^2 \overline{u_x^b} + 2U_x^a \overline{u_x^a\left(u_x^b\right)^2} + 2U_x^b \overline{u_x^b\left(u_x^a\right)^2}\end{aligned} \tag{14}$$

Only the first two terms on the right-hand side of equation (14) will contribute to the jet noise. The three following terms are constant with τ and their derivatives will vanish; the next two terms will likewise vanish, since the components of $\vec{u}$ have zero mean. The last two terms involve triple velocity correlations; it is argued in reference 4, appendix B, that their integral over $\vec{\eta}$-space will vanish for homogeneous isotropic turbulence. These terms would also vanish prior to integration if the turbulence were postulated as a Gaussian process.

On the assumption of normal joint probability for u_x^a and u_x^b, equation (14) becomes (see, e.g., ref. 14)

$$\overline{\left(v_x^a\right)^2\left(v_x^b\right)^2} = 2\left(\overline{u_x^a u_x^b}\right)^2 + 4U_x^a U_x^b\,\overline{u_x^a u_x^b} + \overline{\left(u_x^a\right)^2}\,\overline{\left(u_x^b\right)^2}$$

Self-noise — Shear noise

$$+ \text{Noncontributing terms} \tag{15}$$

The first term has no contribution from the mean flow U: this source term accounts for the "self-noise" of the turbulence alone. The second term ultimately depends on the mean flow shear in its contribution to the jet noise: it is termed the "shear noise." The third term is constant with τ and will vanish on differentiation.

Self-Noise

The contribution of the self-noise to the correlation $R(\vec{x}^a, \vec{x}^b, \tau)$ of sound pressure at the two equidistant points $\vec{x}^a$ and $\vec{x}^b$ with time delay τ (the final evaluation specializes to $\tau = 0$) is now formulated. The first term on the right-hand side of equation (15) – the self-noise term – may be expanded as follows:

$$\left.\begin{aligned} u_x^a &= n_i^a u_i^a, \qquad & u_x^b &= n_j^a u_j^a \\ \overline{u_x^a u_x^b} &= n_i^a n_j^b\,\overline{u_i^a u_j^b} & & \\ 2\left(\overline{u_x^a u_x^b}\right)^2 &= 2n_i^a n_j^b n_k^a n_\ell^b\,\overline{u_i^a u_j^b}\;\overline{u_k^a u_\ell^b} & & \end{aligned}\right\} \tag{16}$$

However, the postulated isotropy of the u_i field may be exploited in order to obtain a simpler expression. To this end, new reference axes are chosen so that the 1-axis lies along $\vec{x}^a$, or $\vec{n}^a$, the orthogonal 2- and 3-axes being arbitrary:

$$\left.\begin{aligned} \begin{bmatrix} n_1^a \\ n_2^a \\ n_3^a \end{bmatrix} \rightarrow \begin{bmatrix} \hat{n}_1^a \\ \hat{n}_2^a \\ \hat{n}_3^a \end{bmatrix} &= \begin{bmatrix} 1 \\ 0 \\ 0 \end{bmatrix} & \qquad \begin{bmatrix} n_1^b \\ n_2^b \\ n_3^b \end{bmatrix} \rightarrow \begin{bmatrix} \hat{n}_1^b \\ \hat{n}_2^b \\ \hat{n}_3^b \end{bmatrix} &= \begin{bmatrix} \cos\psi \\ \sin\psi\cos\mu \\ \sin\psi\sin\mu \end{bmatrix} \end{aligned}\right\} \tag{17}$$

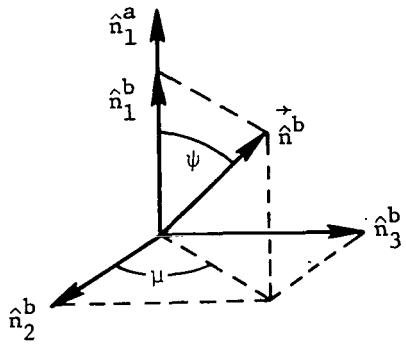

Sketch (a)

Here ψ (polar angle) is the angle between $\vec{x}^a$ and $\vec{x}^b$ (or $\vec{n}^a$ and $\vec{n}^b$) and μ is an azimuth angle. (See sketch (a).) Then

$$\overline{u_x^a u_x^b} = \hat{n}_1^b \overline{u_1^a u_1^b} + \hat{n}_2^b \overline{u_1^a u_2^b} + \hat{n}_3^b \overline{u_1^a u_3^b} \tag{18}$$

$$2\left(\overline{u_x^a u_x^b}\right)^2 = 2\left(\hat{n}_i^b \hat{n}_j^b \overline{u_1^a u_i^b}\ \overline{u_1^a u_j^b}\right) \tag{19}$$

The contribution of unit volume to the correlation (eq. (11)) to be evaluated with the use of equations (15) and (19) should be invariant with the angle μ for fixed ψ when convection effects are neglected: this is a consequence of the postulated isotropy of the turbulence. Thus there should be no change upon averaging over μ. Performing this average on equation (19) with the use of equations (17) results in

$$2\left(\overline{u_x^a u_x^b}\right)^2 = 2\left(\overline{u_1^a u_1^b}\right)^2 \cos^2\psi + \left[\left(\overline{u_1^a u_2^b}\right)^2 + \left(\overline{u_1^a u_3^b}\right)^2\right]\sin^2\psi \tag{20}$$

Following reference 4, it is now postulated that $\overline{u_i^a u_j^b}$ is factorable into a space factor appropriate to homogeneous isotropic turbulence (e.g., Batchelor, ref. 14) and a time factor:

$$\overline{u_i^a u_j^b} = g(\tau_1)\, C_{ij}(\vec{\eta}) \tag{21a}$$

$$g(\tau_1) = e^{-\omega_f |\tau_1|} \tag{21b}$$

$$C_{ij}(\vec{\eta}) = \overline{u_1^2}\left[\left(f + \frac{1}{2}\eta f'\right)\delta_{ij} - \frac{1}{2}f'\frac{\eta_i\eta_j}{\eta}\right] \tag{21c}$$

$$f(\eta) = \exp\left(\frac{-\pi^2\eta^2}{L^2}\right) \qquad \eta^2 = \eta_1^2 + \eta_2^2 + \eta_3^2 \tag{21d}$$

$$f'(\eta) = \frac{df}{d\eta} \tag{21e}$$

More generally, f may be any suitable universal function of η; in the present model of turbulence it is taken to have the form shown, which has been used by Lilley (ref. 15). The longitudinal macroscale is denoted by L.

It is known that the function $\exp\left(-\omega_f|\tau_1|\right)$ – which resembles the results of hot-wire measurements of turbulence – is unacceptable in the vicinity of $\tau_1 = 0$; a zero slope is required there on theoretical grounds. However, experimentally the cusplike shape is observed extremely close to $\tau_1 = 0$; the region of failure is normally too small to be resolved from the measurements. Thus the specification (eqs. (21)) may be regarded as being applicable very, very close to, but not precisely at, $\tau_1 = 0$. The practical effect of this exception for numerical work is negligible. (It may be argued that the foregoing implies a nearly singular behavior of $\partial^4 g/\partial\tau_1^4$ as $\tau_1 \to 0$. However, restoration of the neglected time delay across a correlation volume should largely suppress the effects: τ_1 can then vanish only at a single point within the correlation volume.)

The self-noise contribution to the two-microphone correlation is obtained by inserting the first term of equation (15) into equation (11). Then with the use of equations (20) and (21), there results

$$R_{se}(\vec{x}^a, \vec{x}^b, \tau) = \rho_o^2\left(\pi^2 c_o^4 x^2\right)^{-1} \iint \omega_f^4 e^{-2\omega_f|\tau+\Delta|}$$

$$\times \left\{2C_{11}^2(\vec{\eta})\cos^2\psi + \left[C_{12}^2(\vec{\eta}) + C_{13}^2(\vec{\eta})\right]\sin^2\psi\right\} d^3\vec{\eta}\, d^3\vec{Y} \tag{22}$$

where the retarded time difference $\tau + \Delta$ has been inserted for τ_1.

An approximation may be made to decouple and simplify the $\vec{\eta}$ and $\vec{Y}$ integrals. In the expression for Δ (eq. (8)), involving both $\vec{\eta}$ and $\vec{Y}$, the term in $\vec{\eta}$ accounts for phase incoherence in the source region. Suppose the coherent regions, or "eddies,"

are taken to be acoustically compact (small compared with a typical wavelength of the radiated sound), then this term – in the postulated absence of convection – may be neglected. (An equivalent assumption has been made in the work of Lighthill (ref. 9) and others.) Equation (8) then reduces to

$$\Delta \approx \frac{\vec{Y} \cdot \left(\vec{n}^a - \vec{n}^b\right)}{c_o} \tag{23}$$

In this approximation Δ is the difference in travel times of sound from a source point at $\vec{Y}$ – the centroid of an "eddy," or correlation volume – to field points at $\vec{x}^a$ and $\vec{x}^b$, respectively. The assumption of acoustic compactness, it is noted, is limited to the eddies: the total volume occupied by these eddies is not taken to be compact.

Evaluation of the inner integrals in equation (22) covering all $\vec{\eta}$-space is elementary, but a little tedious, and yields

$$R_{se}\left(\vec{x}^a, \vec{x}^b, \tau\right) = \frac{\rho_o^2}{2^{3/2}\pi^2 c_o^4 x^2}\left(\frac{1}{8} + \frac{7}{8}\cos^2\psi\right) \int_{jet} \left(\overline{u_1^2}\right)^2 L^3 \omega_f^4 e^{-2\omega_f|\tau+\Delta|}\, d^3\vec{Y} \tag{24}$$

The remaining integral may be limited to the volume occupied by the jet, since $\overline{u_1^2} \to 0$ outside the nominal jet boundary.

It often suffices to avoid the integration in $\vec{Y}$ and look merely at the integrand in equation (24): this is the contribution to R_{se} from unit volume of the jet. It was earlier remarked that the directional properties of the mean-square sound pressure emitted from a unit volume of a jet are fairly representative of those of the entire jet in a given (corresponding) narrow frequency band. However, no such simple correspondence is applicable to the two-point correlation of sound pressure, for reasons brought out below. Thus, the threefold integrals that largely sufficed for the single-microphone case must give way to a sixfold integral for the two-microphone case. Accordingly, the $\vec{Y}$ integration in equation (24) will have to be carried out.

Suppose, just for the moment, that the major noise-producing region of the jet is postulated to be acoustically compact (and to contain the origin of coordinates) – that is, its dimensions are much less than the typical wavelength of the generated sound – then differences in travel times Δ are negligible in equation (24). In this case, the integral will reduce to a simple nondirectional factor. The factor $(1/8 + 7/8 \cos^2\psi)$ is thus the directivity of R_{se} for an acoustically compact jet. The integral, when Δ is not neglected, is therefore a multiplicative factor that allows for noncompactness of the jet. Note that it is not unreasonable for certain purposes to assume – as has been done here –

that the correlation volumes are compact; but it is totally unrealistic to assume that the many times larger jet is compact.

Integral Over Noncompact Jet

From equation (23) it can be seen that

$$c_0\Delta \approx \vec{Y} \cdot \vec{n}^a - \vec{Y} \cdot \vec{n}^b$$

measures the difference in distance from $\vec{Y}$ (center of an "eddy") to points $\vec{x}^a$ and $\vec{x}^b$; hence Δ measures the difference in travel times for sound originating from the eddy.

This time difference reduces the cross-correlation of signals received at $\vec{x}^a$ and $\vec{x}^b$ in precisely the same fashion as time delay reduces the autocorrelation of a single signal (at $\vec{x}^a$, say). This is apparent from the way Δ appears along with τ in the exponential in equation (24). Thus the noncompactness factor can have a powerful effect in modifying the directional two-point correlation pattern predicted for a compact jet when Δ is large.

Assume that the major contribution to R_{se} comes from the jet mixing region and limit the integral in equation (24) to that region. On abbreviating the integrand as $G(\vec{Y})$ and going over to cylindrical coordinates, the integral takes the form

$$\iiint_{jet} Gr\, dr\, d\gamma\, dY_1 \tag{25}$$

which can be transformed into

$$\iiint_{jet} GrY_1\, dY_1\, d\gamma\, d\left(\frac{r-R}{Y_1}\right) \tag{26}$$

The scale L and characteristic radian frequency ω_f depend essentially on Y_1 alone, and

$$\overline{u_1^2}(\vec{Y}) = \overline{u_1^2}(R)\, F\left(\frac{r-R}{Y_1}\right) \tag{27}$$

describes the turbulent velocity in the spreading annular mixing region: it specifies similar radial profiles at successive axial distances. To the present accuracy the part of the integral in equation (24) varying with r is just

$$\int_{-R/Y_1}^{\infty} rF^2\left(\frac{r-R}{Y_1}\right) d\left(\frac{r-R}{Y_1}\right) \tag{28}$$

Since F peaks strongly at $r = R$, this is approximately Rg_1, where g_1 is a pure number. Additionally, although ω_f and L vary with Y_1, their product is essentially invariant (constant Strouhal number).

Thus the correlation (eq. (24)) reduces to

$$R_{se}\left(\vec{x}^a, \vec{x}^b, \tau\right) = \frac{\rho_o{}^2 g_1 \left(\omega_f L\right)^4 R\left[\overline{u_1{}^2}(R)\right]^2}{2^{3/2}\pi^2 c_o{}^4 x^2}\left(\frac{1}{8} + \frac{7}{8}\cos^2\psi\right)$$

$$\times \int_0^{\ell} \frac{Y_1}{L} dY_1 \int_0^{2\pi} e^{-2\omega_f|\tau+\Delta|} d\gamma \tag{29}$$

where ℓ is the effective length of the source region. An approximation to the mean of diverse hot-wire measurements is the linear dependence $L = Y_1/g_2$, where g_2 is a constant of order 5 to 10. Accordingly, the correlation may be written as

$$R_{se}\left(\vec{x}^a, \vec{x}^b, \tau\right) = \frac{2\pi\rho_o{}^2 g_1 g_2 \left(\omega_f L\right)^4 R\ell\left[\overline{u_1{}^2}(R)\right]^2}{2^{3/2}\pi^2 c_o{}^4 x^2}\left(\frac{1}{8} + \frac{7}{8}\cos^2\psi\right)$$

$$\times \frac{1}{\ell}\int_0^{\ell} dY_1 \frac{1}{2\pi}\int_0^{2\pi} e^{-2\omega_f|\tau+\Delta|} d\gamma \tag{30}$$

For evaluation, a suitable expression for the difference in travel times Δ is required. Spherical polar coordinates are introduced for $\vec{n}^a$ and $\vec{n}^b$ and the cylindrical coordinates for $\vec{Y}$ are recalled:

$$\left.\begin{aligned} Y_1 &= Y_1 & n_1^a &= \frac{x_1^a}{x} = \cos\theta_a \\ Y_2 &= r\cos\gamma & n_2^a &= \frac{x_2^a}{x} = \sin\theta_a\cos\varphi_a \\ Y_3 &= r\sin\gamma & n_3^a &= \frac{x_3^a}{x} = \sin\theta_a\sin\varphi_a \end{aligned}\right\} \tag{31}$$

with similar expressions for $\left(n_1^b, n_2^b, n_3^b\right)$.

It has already been noted that $F(r)$ in equation (27) peaks very sharply at $r = R$. This implies that the sources of sound are concentrated in the neighborhood of the cylinder $r = R$. The expression for Δ is therefore simplified with very little error in final results by replacing r by R in equations (31). Then Δ may be expanded as

$$c_o\Delta = \vec{Y} \cdot \left(\vec{n}^a - \vec{n}^b\right) = Y_1\left(\cos\theta_a - \cos\theta_b\right) + R\cos\gamma\left(\sin\theta_a\cos\varphi_a - \sin\theta_b\cos\varphi_b\right) + R\sin\gamma\left(\sin\theta_a\sin\varphi_a - \sin\theta_b\sin\varphi_b\right) \tag{32}$$

This reduces to different forms for the two special cases under consideration (fig. 6): (1) the two microphones lie on a circle of latitude $\theta_a = \theta_b$ and (2) the two microphones lie on a meridian circle $\varphi_a = \varphi_b$. Note that the polar angles θ_a, θ_b are measured from the jet axis.

The double integral in equation (30) is evaluated in appendixes B and C for cases I and II, respectively, by using certain simplifying assumptions. The evaluation is limited to the special case $\tau = 0$. (That is, the time delay of signal reception between the two microphones is specified to be zero.) Insertion of the final results into equation (30) gives

Case I: $\theta_a = \theta_b$; $\varphi_a = 0$

$$\left.\begin{aligned} R_{se}\left(\vec{x}^a, \vec{x}^b, 0\right) &= \frac{g_1 g_2 \rho_o^2}{2^{1/2}\pi}\left(\frac{\omega_f L}{c_o}\right)^4 \frac{\left(\overline{u_1^2}\right)^2 R\ell}{x^2}\left(\frac{1}{8} + \frac{7}{8}\cos^2\psi\right) I\left(q_{se}\right) \\ I\left(q_{se}\right) &= \frac{2}{\pi}\int_0^{\pi/2} e^{-q_{se}\sin\epsilon}\, d\epsilon = \text{Noncompactness factor} \\ q_{se} &= 4\left\langle\omega_f\right\rangle\left(R/c_o\right)\left|\sin\theta_b \sin\frac{\varphi_b}{2}\right| \end{aligned}\right\} \tag{33}$$

Case II: $\varphi_a = \varphi_b = 0$

$$R_{se}\left(\vec{x}^a, \vec{x}^b, 0\right) = \frac{g_1 g_2 \rho_o^2}{2^{1/2}\pi}\left(\frac{\omega_f L}{c_o}\right)^4 \frac{\left(\overline{u_1^2}\right)^2 R\ell}{x^2}$$

$$\times \left[\frac{1}{8} + \frac{7}{8}\cos^2\left(\theta_b - \theta_a\right)\right]\frac{\left(1 - e^{-2\delta}\right)}{2\delta} \qquad (34)$$

Noncompactness factor

where

$$\delta = \frac{\ell\left\langle\omega_f\right\rangle}{c_o}\left|\cos\theta_b - \cos\theta_a\right|$$

In both cases $\left\langle\omega_f\right\rangle$ signifies an effective average of ω_f over the length ℓ of the mixing region (appendix B). Equations (34) become invalid near $\theta_b \approx -\theta_a$ and for that subcase are to be replaced by equations (33) with $\theta_b = \theta_a$, $\varphi_b = 180^o$.

Shear Noise

The shear-noise contribution to the two-microphone correlation is obtained by replacing $\overline{\left(v_x^a\right)^2\left(v_x^b\right)^2}$ in equation (11) by the second term of its expansion in equation (15), namely, $4U_x^a U_x^b \overline{u_x^a u_x^b}$. Again, reference 4 is followed in describing the mean flow shear by the correlation

$$U\left(\vec{Y} + \frac{\vec{\eta}_n}{2}\right)U'\left(\vec{Y} - \frac{\vec{\eta}_n}{2}\right) \equiv UU'\left(\vec{\eta}_n, \vec{Y}\right) = U^2\left(\vec{Y}\right)e^{-\sigma\pi\eta_n^2/L^2} \qquad (35)$$

where the prime designates the second point, $\vec{\eta}_n$ is measured radially outward, and the flow is treated as locally planar within a correlation volume; correspondingly,

$$U_x^a U_x^b = U^2\left(\vec{Y}\right)n_1^a n_1^b e^{-\sigma\pi\eta_n^2/L^2} \qquad (36)$$

For $\overline{u_x^a u_x^b} = n_i^a n_j^b \overline{u_i^a u_j^b}$, it is again specified that $\overline{u_i^a u_j^b}$ has the form $C_{ij}\left(\vec{\eta}\right)g(\tau)$, which is spelled out more fully in equations (21). Putting this all together gives the source term as

$$\frac{\partial^4}{\partial \tau^4} 4U_x^a U_x^b \overline{u_x^a u_x^b} = 4n_1^a n_1^b n_i^a n_j^b \overline{u_1^2}\, U^2(\vec{Y}) \omega_f^4 e^{-\omega_f|\tau_1|} C_{ij}(\vec{\eta}) e^{-\sigma\pi\eta_n^2/L^2} \tag{37}$$

This is to be inserted in equation (11) and evaluated at $\tau_1 = \tau + \Delta$ to yield the two-microphone correlation. Specializing to the simplest case, $\tau = 0$, gives

$$R_{sh}(\vec{x}^a, \vec{x}^b, 0) = \frac{n_1^a n_1^b n_i^a n_j^b \rho_o^2}{4\pi^2 c_o^4 x^2} \iint \omega_f^4 e^{-\omega_f|\Delta|} U^2(\vec{Y})\, \overline{u_1^2}(\vec{Y}) \times C_{ij}(\vec{\eta}) e^{-\sigma\pi\eta_n^2/L^2}\, d^3\vec{\eta}\, d^3\vec{Y} \tag{38}$$

For reasons related to the axisymmetry, cylindrical coordinates $\vec{Y} = Y_1, r, \gamma$ will now be used to locate the volume element $d^3\vec{Y}$. The integral in $\vec{\eta}$-space will be simplified if the coordinate axes are rotated counterclockwise through angle γ $(\vec{\eta} \to \hat{\vec{\eta}})$; then the radial two-point separation η_n will become $\hat{\eta}_2$, but the $C_{ij}(\hat{\eta})$ will be unchanged in form because of the postulated isotropy of the turbulence. All but two of the C_{ij} terms will have zero integrals; the surviving integrals are

$$\int_\infty C_{11}(\hat{\vec{\eta}}) e^{-\sigma\pi\hat{\eta}_2^2/L^2}\, d^3\hat{\vec{\eta}} = \int_\infty C_{33}(\hat{\vec{\eta}}) e^{-\sigma\pi\hat{\eta}_2^2/L^2}\, d^3\hat{\vec{\eta}} = \frac{L^3\sigma}{2(1+\sigma)^{3/2}} \tag{39}$$

Upon insertion of equations (31) referred to the rotated axes $(\varphi \to \hat{\varphi})$, along with equation (39), and noting that $\overline{u_1^2(\vec{Y})}$ vanishes outside the jet, equation (38) reduces to

$$R_{sh}(\vec{x}^a, \vec{x}^b, 0) = \frac{\rho_o^2 \sigma}{8\pi^2 c_o^4 x^2 (1+\sigma)^{3/2}} \int_{jet} \left(\cos^2\theta_a \cos^2\theta_b + \frac{1}{2}\cos\theta_a \cos\theta_b \sin\theta_a \sin\theta_b \times \sin\hat{\varphi}_a \sin\hat{\varphi}_b\right) \overline{u_1^2} L^3 \omega_f^4 e^{-\omega_f|\Delta|} U^2(\vec{Y})\, d^3\vec{Y} \tag{40}$$

Reversion to the original reference axes gives, on noting that $\hat{\varphi}_a$ and $\hat{\varphi}_b$ are angular deviations from the angle γ orienting the volume element,

$$R_{sh}\left(\vec{x}^a,\vec{x}^b,0\right) = \frac{\rho_o{}^2\sigma}{8\pi^2 c_o{}^4 x^2(1+\sigma)^{3/2}} \int_{jet} \Big[\cos^2\theta_a \cos^2\theta_b + \frac{1}{2}\cos\theta_a \cos\theta_b \sin\theta_a \sin\theta_b$$

$$\times \sin\left(\varphi_a - \gamma\right) \sin\left(\varphi_b - \gamma\right)\Big] \overline{u_1^2}\, L^3 \omega_f{}^4 e^{-\omega_f|\Delta|} U^2\left(\vec{Y}\right) d^3\vec{Y} \qquad (41)$$

Just as for the self-noise let

$$\int_{jet} G\left(\vec{Y}\right) d^3\vec{Y} = \iiint_{jet} GrY_1\, dY_1\, d\gamma\, d\left(\frac{r-R}{Y_1}\right)$$

(eq. (26)) and invoke the same similarity assumptions concerning L, ω_f, and $\overline{u_1^2}$ leading to equation (30). Additionally, the specification $\varphi_a = 0$ can be made without loss of generality: φ_b will take on the role of $\varphi_b - \varphi_a$ because of the axisymmetry. With these stipulations together with $\overline{u_1^2} = \overline{u_1^2}(R)\, F\left[(r-R)/Y_1\right]$ and $U^2 = \text{Constant}$ (annular mixing region), equation (41) reduces after the radial integration to

$$R_{sh}\left(\vec{x}^a,\vec{x}^b,0\right) = \frac{\left(\omega_f L\right)^4 R\ell\, U^2\, \overline{u_1^2}(R)\sigma}{8\pi^2 c_o{}^4 x^2(1+\sigma)^{3/2}} \frac{1}{\ell}\int_0^{\ell} dY_1 \int_0^{2\pi} \Big[\cos^2\theta_a \cos^2\theta_b$$

$$+ \cos\theta_a \cos\theta_b \sin\theta_a \sin\theta_b \sin\left(\gamma - \varphi_b\right) \sin\gamma\Big] e^{-\omega_f|\Delta|}\, d\gamma \qquad (42)$$

where

$$g_2 = Y_1/L = \text{Number} \quad \text{(scaling law)}$$

$$g_3 = \int_{-R/Y_1}^{\infty} F\left(\frac{r-R}{Y_1}\right) d\left(\frac{r-R}{Y_1}\right) = \text{Number} \quad (\text{since } F = 0 \text{ at lower limit})$$

and $\Delta\left(\gamma;\ \theta_a,\theta_b,\varphi_b\right)$ is defined in equation (32).

The experimental evidence indicates that the compactness condition $\left(\omega_f|\Delta| \leqq 4\pi R/\lambda << 1\right)$ is not normally met. Thus the exponential in equation (42) that accounts for noncompactness of the source region (cf. earlier discussion regarding self-noise) must be retained. The integration is discussed in appendix D. The rather lengthy

results for the shear-noise correlation $R_{sh}(\vec{x}^a, \vec{x}^b, 0)$ will not be repeated here. Instead, the combined contributions of self-noise plus shear noise will be summarized in the following section.

Summarized Predictions

In order to put the final equations in the most compact form, a normalization procedure is used. It is observed that the correlation $R(\vec{x}^a, \vec{x}^b) \equiv \overline{p_a p_b}$ becomes merely $\overline{p^2}(\vec{x}^a)$ when $\vec{x}^b = \vec{x}^a$. On specializing to the self-noise, the correlation in equations (33) reduces to

$$R_{se}(\vec{x}^a, \vec{x}^a, 0) = \overline{p_{se}^2} = \frac{\rho_o^2 \ell^2 \Omega}{2^{1/2}\pi} \left(\frac{\omega_f L}{c_o}\right)^4 \frac{\left(\overline{u_1^2}\right)^2 R\ell}{x^2} \tag{43}$$

A similar reduction occurs for the shear-noise correlation when $\vec{x}^b = \vec{x}^a$; the maximum value occurs with $\vec{x}^a$ oriented along the jet axis ($\theta = 0$):

$$R_{sh}(\vec{x}^a, \vec{x}^a, 0)_{max} = \left(\overline{p_{sh}^2}\right)_{max} = \frac{\rho_o^2 \ell^2}{4\pi} \left(\frac{\omega_f L}{c_o}\right)^4 \frac{\overline{u_1^2} U^2 R\ell\sigma}{x^2(1+\sigma)^{3/2}} \tag{44}$$

The ratio of the peak shear-noise intensity to the self-noise intensity is a pure number:

$$\frac{\beta}{2} = \frac{\left(\overline{p_{sh}^2}\right)_{max}}{\overline{p_{se}^2}} = 2^{-3/2} \frac{g_3}{g_1} \frac{U^2}{\overline{u_1^2}} \frac{\sigma}{(1+\sigma)^{3/2}} \tag{45}$$

When the integrals g_1 and g_3 over the jet radius are replaced by unity, equation (45) reduces to the corresponding ratio B/A referred to unit volume given in reference 4. The parameter σ in equation (45) is evaluated in terms of the mean flow shear $\partial U/\partial r$ in appendix B of reference 5.

The final equations for the combined contributions of self-noise and shear noise to the two-microphone correlation

$$R(\vec{x}^a, \vec{x}^b, 0) = R_{se}(\vec{x}^a, \vec{x}^b, 0) + R_{sh}(\vec{x}^a, \vec{x}^b, 0)$$

are expressed in terms of $\overline{p_{se}^2}$. For the two cases of main interest (fig. 6), the equations are

Case I: $\theta_a = \theta_b = \theta, \quad \varphi_a = 0$

$$\left.\begin{aligned}
\frac{R\left(\vec{x}^a, \vec{x}^b, 0\right)}{p_{se}^2} &= \left(\frac{1}{8} + \frac{7}{8}\cos^2\psi\right) I\left(q_{se}\right) + \frac{\beta}{4}\left(\cos^4\theta + \cos^2\theta \cos\psi\right) I\left(q_{sh}\right) \\
&\quad - \frac{\beta}{4}\cos^2\theta \sin^2\theta \left[I\left(q_{sh}\right) - J\left(q_{sh}\right)\right]
\end{aligned}\right\} \tag{46}$$

where

$$\left.\begin{aligned}
I(q) &= \frac{2}{\pi}\int_0^{\pi/2} e^{-q \sin\epsilon}\, d\epsilon \\
J(q) &= \frac{4}{\pi}\int_0^{\pi/2} \left(\sin^2\epsilon\right) e^{-q \sin\epsilon}\, d\epsilon
\end{aligned}\right\} \quad \text{Noncompactness factors}$$

$$\left.\begin{matrix} q_{se} \\ q_{sh} \end{matrix}\right\} = \left.\begin{matrix} 4 \\ 2 \end{matrix}\right\} \left\langle \omega_f \right\rangle \left(R/c_o\right) \left| \sin\theta \sin\frac{\varphi_b}{2} \right|$$

$\left\langle \omega_f \right\rangle$ = Effective average of ω_f over mixing region

ψ = Angle between $\vec{x}^a$ and $\vec{x}^b$

$= \cos^{-1}\left(\cos^2\theta + \sin^2\theta \cos\varphi_b\right)$

The noncompactness integrals $I(q)$ and $J(q)$ are functions of θ and φ_b that are readily evaluated numerically by computer. For fixed θ they approximate roughly to the form $e^{-\text{const}\left|\varphi_b\right|}$, the constant depending on θ.

Case II: $\varphi_b = \varphi_a$

$$\begin{aligned}
\frac{R\left(\vec{x}^a, \vec{x}^b, 0\right)}{p_{se}^2} &= \frac{1 - e^{-2\delta}}{2\delta}\left[\frac{1}{8} + \frac{7}{8}\cos^2\left(\theta_b - \theta_a\right)\right] \\
&\quad + \frac{\beta}{2}\frac{1 - e^{-\delta}}{\delta}\left(\cos^2\theta_a \cos^2\theta_b + \frac{1}{2}\cos\theta_a \cos\theta_b \sin\theta_a \sin\theta_b\right)
\end{aligned} \tag{47a}$$

where

$$\delta = \left(\frac{\langle \omega_f \rangle \ell}{c_o}\right) \left| \cos \theta_b - \cos \theta_a \right| \tag{47b}$$

(Eqs. (47) are invalid in the vicinity of $\theta_b = -\theta_a$ and are to be replaced there by eqs. (46) with $\varphi_b = 180^o$; cf. footnote 2, p. 37.) The noncompactness factors in this case are $\left(1 - e^{-2\delta}\right)/2\delta$ and $\left(1 - e^{-\delta}\right)/\delta$; they again have an angular dependence with a cusp as $\vec{x}^b \to \vec{x}^a$ (or as $\theta_b \to \theta_a$).

DISCUSSION

Comparison With Experiments of Maestrello

The theoretical equations for the two-microphone correlation

$$\overline{p_a(\vec{x}^a,t)p_b(\vec{x}^b,t)} \equiv R(\vec{x}^a,\vec{x}^b,0)$$

are given in equations (46) and (47), with ancillary definitions in equations (43) to (45). The correlations are nondimensionalized by division by the mean-square self-noise sound pressure $\overline{p_{se}^2}$ to simplify the expressions. However, it is preferable to use the more usual scheme of normalization:

$$\frac{\overline{p_a p_b}}{\sqrt{\overline{p_a}^2\,\overline{p_b}^2}} = \frac{R(\vec{x}^a,\vec{x}^b,0)}{\sqrt{R(\vec{x}^a,\vec{x}^a,0)\,R(\vec{x}^b,\vec{x}^b,0)}} \tag{48}$$

The values of R may be taken from equations (46) and (47) as the case may be, and it will be noted that $\overline{p_{se}^2}$ will cancel out.

The normalization (eq. (48)) corrects for large amplitude changes resulting from convection and refraction effects excluded from the theory. To the extent that they could be approximated as uncorrelated multiplicative factors for p_a and p_b herein, they would cancel out along with $\overline{p_{se}^2}$.

The governing parameters in the equations are $2\langle \omega_f \rangle R/c_o$ for case I $(\theta_b = \theta_a = \theta)$ and $\langle \omega_f \rangle \ell/c_o$ for case II $(\varphi_b = \varphi_a)$. In terms of Strouhal number $N_{Str} \equiv f_f D/U_j$, these take the respective forms $2\pi M_j \langle N_{Str} \rangle$ for case I and $2\pi M_j (\ell/D) \langle N_{Str} \rangle$ for case II. Here D is the jet diameter, ℓ is the effective length of the noise-generating "cylinder,"

and the angular brackets indicate an effective average over length ℓ. The ratio ℓ/D was taken as 5.25, about the length of the mixing region. Mach number enters indirectly through its influence on $\langle N_{Str} \rangle$ as well as directly; the effects may be opposing. For numerical application of the theory at $M_j = 0.75$, $\langle N_{Str} \rangle$ was taken as 0.40. This was frankly chosen for best fit to the experimental data, but the value is compatible with turbulence correlation data.

The turbulence data of reference 16 may be drawn on to elaborate the last remark. An appropriate autocorrelation is one referred to a reference frame moving with the local convection velocity. This moving-frame autocorrelation is the envelope of two-point correlations measured in the fixed (laboratory) frame (ref. 16). These envelope autocorrelations in reference 16 and elsewhere roughly resemble the simple exponential choice for $g(\tau)$ herein, but they deviate at small τ and show a sharp upturn as $\tau \to 0$. Thus the experimental correlations are better fitted by the sum of two exponentials: one with fast decay to dominate the slope and higher derivatives for small τ plus another to dominate at large τ.

Now the key features of the theory are displayed at small τ (including the cusp at $\tau = 0$); hence, since the theory (in its present version) is limited to a single exponential, it is appropriate to choose the exponent for best fit to the experimental moving-frame autocorrelations in the region of small τ. This has been done with the envelope curve of figure 21a of reference 16, which is a plot of $\overline{u_1^a u_1^b}\left(U_j\tau/D\right)$ for $\vec{\eta} = 0$ in the present notation; the measurements are made at $Y_1/D = 4.5$ and $r/R = 1.0$, with $M_j \approx 0.13$. The fit is made to the dashed portion of the curve at small τ terminating in the point $U_j\tau/D = 0.065$, $\overline{u_1^a u_1^b} = 0.871$; thus $e^{-\omega_f|\tau|}$ is chosen to pass through this terminal point. The result, with $f_f = \omega_f/2\pi$, is

$$f_f D/U_j \equiv N_{Str} = 0.337 \qquad \left(Y_1/D = 4.5\right) \tag{49}$$

This is to be compared with

$$\left\langle f_f D/U_j \right\rangle \equiv \langle N_{Str} \rangle = 0.400 \qquad \left(Y_1/D \text{ averaged from 0 to } 5.25\right) \tag{50}$$

used in the theory. Since N_{Str} increases with decreasing Y_1/D, the two values are quite compatible.

Values of $f_f D/U_j$ quoted in the literature (cf., e.g., ref. 3, p. 120) are obtained in a fashion that is different and not appropriate to the present choice for the theory. They

do not result from a fit to the experimental autocorrelation at small τ. Instead, $\omega_f = 2\pi f_f$ is chosen as the reciprocal of the time-scale: the integral of the autocorrelation. This yields manyfold smaller values of f_f.

Experimental measurements of the two-microphone correlations are available from a massive and definitive investigation by Maestrello (ref. 7). Only a few of his results are drawn on for the comparison. In particular, attention is limited to the peak values of the correlations when plotted against time delay τ. In the predictions of the theory these peaks occur at $\tau = 0$. In the experimental measurements the peaks are essentially at $\tau = 0$ for the axisymmetric case I (explained in fig. 6), but are somewhat offset from $\tau = 0$ for the nonsymmetric case II (fig. 6), owing to convection and refraction effects excluded from the theory.

Refer once again to figure 6 to see clearly the two main cases of microphone positioning. In case I both microphone position vectors $\vec{x}^a$ (to p_a) and $\vec{x}^b$ (to p_b) lie on a cone ($\theta_a = \theta_b = \theta$; $\varphi_a = 0$, φ_b varies). In case II, the vectors $\vec{x}^a$ (to p_a) and $\vec{x}^b$ (to p_b) lie in the plane of the jet and p_a and p_b move around a meridian circle (p_a at θ_a, p_b at θ_b).

Example polar plots of Maestrello's experimental measurements (ref. 7) are shown in figure 7 for case I ($\theta_a = \theta_b = \theta$; $\varphi_a = 0$, φ_b varies) at Mach number $M_j = 0.75$: the normalized two-microphone correlation is plotted against the azimuthal separation φ_b of the microphones. These and other cases are replotted in Cartesian format and compared with predictions of the present theory in figures 8 to 11. The general shape of the experimental curves, in particular the cusp at $\varphi_b = 0$, is well predicted. Quantitatively the agreement is reasonably good in the downstream quadrant (fig. 8), excellent in the 90^o plane (fig. 9), and only fair in the upstream quadrant (fig. 10). It is significant that the theory, which omits convection and refraction effects, is most accurate in the 90^o plane, where such effects should be minimal.

An additional factor presumably contributing slightly to the accuracy at 90^o is the vanishing there of the slightly uncertain amount of shear-noise contribution. In the specifications herein for the theory there is a parameter $\beta/2$ = Peak shear-noise intensity/Self-noise intensity. Values of β inferred from single-microphone measurements of jet noise vary from 1.58 to 3.55 (ref. 5); the theoretically based value $\beta = 2.0$ was used herein, except where otherwise specified.

To elucidate the significance of the shear-noise/self-noise ratio $\beta/2$ further, the effects of three different values were explored: theoretical curves for $\beta = 0$, 2.0, and 3.55 were evaluated for case I with $\theta = 30^o$ and 60^o. These are presented in figure 11, along with Maestrello's measurements. The choices $\beta = 2.0$ and $\beta = 3.55$ give comparably good agreement with experimental results at both $\theta = 30^o$ and $\theta = 60^o$.

On the other hand, the choice $\beta = 0$ (no shear noise) considerably degrades the agreement at $\theta = 30^{o}$. Thus the shear noise cannot be ignored, but the results are not highly sensitive to its precise proportion, except that values of β much below 2 must be ruled out. Put another way, the results are not highly sensitive to the basic directivity resulting from the "nature of the sources" referred to in figure 4.

The agreement between the theoretical curves and the experimental values in the upstream quadrant $\theta > 90^{o}$ (fig. 10) is substantially poorer than in the downstream quadrant $\theta < 90^{o}$ (fig. 8). In particular, the progression with increasing θ is wrong. This can be explained qualitatively in terms of convection and flow-shrouding effects omitted from the theory. A crude accounting for these Doppler effects predicts changes in the effective difference in travel times Δ to the two microphones: it seems that a corrected Δ would be smaller than that of equations (32) for $\theta < 90^{o}$ and larger for $\theta > 90^{o}$. Such changes are in the direction to improve agreement with experiment.

Polar plots of Maestrello's experimental correlations for case II $(\varphi_b = \varphi_a;$ θ_a fixed, θ_b varies$)$ are shown in figure 12 $(M_j = 0.75)$. These are replotted in Cartesian format and compared with theory in figure 13. The agreement for $\theta_a = 60^{o}$ and 120^{o} is seen to be excellent for moderate values of $|\theta_b - \theta_a|$. For $\theta_a = 30^{o}$ the agreement is again excellent in the range $30^{o} \leqq \theta_b < 60^{o}$, but the theory breaks down badly in the range $-30^{o} \leqq \theta_b < 30^{o}$. The breakdown here is not unexpected, since this range defines the "refraction valley"; within this valley refraction effects, excluded from the theory, become dominant as $\theta_b \to 0$.

More explicitly, within the range $-20^{o} < \theta_b < 20^{o}$ the experimental correlations show a deep dip unmatched by the theoretical curves. The loss in correlation is thus associated with those quasi-axial sound rays that have long paths through the jet turbulence. It may be speculated that phase modulation by the turbulence (that is, line broadening) accounts for the extra loss of coherence represented by this dip.

Maestrello's measured correlations at Mach numbers of 0.59, 0.88, and 1.00 (ref. 7) were broadly similar to those at $M_j = 0.75$, but with substantial individual variations. No quantitative attempt was made to apply the theory at these other Mach numbers. Since M_j is not a direct parameter of the theory, the only significant free parameter that may reflect an influence of M_j is the Strouhal number $\langle f_f D/U_j \rangle$. Thus one could vary $\langle f_f D/U_j \rangle$ from the value 0.40 used for $M_j = 0.75$ to different values in attempting to make calculations for different Mach numbers.

Qualitatively it would seem that the agreement with Maestrello's results, with $\langle f_f D/U_j \rangle$ chosen for best fit, will be degraded at the higher Mach numbers. It is the author's view that convection, refraction, and diffraction effects, omitted from the theory, are largely responsible for this; these effects, of course, increase progressively with

Mach number. Another view has been suggested by Maestrello. He attributes the deviations with Mach number to the term in $\vec{\eta}$ in the time-delay equation (eq. (8)); that term – neglected herein for mathematical simplicity – accounts for sound travel time across an "eddy."

Further Considerations

The theory developed herein is not exact: it embodies a number of simplifying assumptions. The extent of agreement with experimental results must therefore be assessed in the light of these approximations. It is worth taking a closer look at some of the approximations at this point; to this end, the statement of assumptions in the Introduction is amplified in the following paragraphs.

Flow refractive effects are suppressed because the governing equation – the Lighthill equation – is not a convected-wave equation. Convection of the sources is likewise not accounted for. The major contribution of these effects is thought to cancel on nondimensionalizing $\overline{p_a p_b}$ by $\sqrt{\overline{p_a{}^2}\,\overline{p_b{}^2}}$. That is, although convection and other flow effects can powerfully affect p_a and p_b, these effects are expected to have rather similar multiplicative effects in the numerator and denominator.

The multipliers resulting from flow effects will not, however, cancel exactly. Put another way, the flow effects will alter the predicted nondimensional correlation somewhat. This comes about because both the source and sound wave convection by the flow will alter the effective difference in travel times Δ to the two microphones. As mentioned earlier, a rough assessment of these changes seems to be in the direction to improve the agreement with experiment.

Another principal limitation is the modeling of the two-point space-time correlations of turbulence $\overline{u_i^a u_j^b}$. These govern the character of the source terms in the Lighthill equation. The functional form assumed in equations (21) embodies certain simplifying assumptions: chiefly the assumption of isotropic turbulence and a specific fashion $g(\tau)$ in which time delay τ enters. The selection of $g(\tau)$ as a multiplicative factor greatly simplifies the mathematics, but it is bound to be an oversimplification. And the choice of $g(\tau)$ as a simple exponential decay in equations (21) approximates the general form of the hot-wire measurements of $\overline{u_i^a u_j^b}(\tau)$ autocorrelations (referred to the convected reference frame), but not the detailed shape, as discussed earlier.

The defects in the chosen $g(\tau)$, which is $e^{-\omega_f|\tau|}$, become apparent when the microphones at $\vec{x}^b$ and $\vec{x}^a$ are brought together; then $R(\vec{x}^a, \vec{x}^b, \tau)$ becomes the autocorrelation $R(\vec{x}^a, \vec{x}^a, \tau)$. The time difference Δ in equation (30) vanishes and $e^{-2\langle\omega_f\rangle|\tau|}$ – an average over the jet – comes outside the integral; this will define the

shape of the self-noise autocorrelation. Similarly, one would obtain $e^{-\omega_f|\tau|}$ for the shear-noise autocorrelation. (In the general case, the predicted autocorrelation is proportional to $\partial^4 g^2(\tau)/\partial\tau^4$ for the self-noise and to $\partial^4 g(\tau)/\partial\tau^4$ for the shear noise.)

A typical measured autocorrelation from Maestrello's investigation (ref. 7) is the curve labeled $\varphi_b = 0^o$ in figure 14. It does resemble $e^{-\langle\omega_f\rangle|\tau|}$ for moderate τ, but for large τ it has a negative loop. Working backward from this, it could be argued that $g(\tau)$ should be chosen so that the derived autocorrelation (which for $\theta \neq 90^o$ is a composite of $\partial^4 g/\partial\tau^4$ and $\partial^4 g^2/\partial\tau^4$) should match the experimental autocorrelation in having a negative loop. The new $g(\tau)$ then becomes $g(\tau + \Delta)$ in the formulas of the theory. With this replacement the negative excursions of figures 7 and other figures would seem to have an explanation: the negative loops in $g(\tau)$ would map into the negative values of $\overline{p_a p_b}$ as Δ maps into φ_b.

The scenario of the last paragraph is, however, oversimplified. The time factor $g(\tau)$ refers to unit volume of the jet turbulence, whereas the measured autocorrelation refers to an average over the jet. The spectrum from unit volume – of which $\partial^4 g(\tau)/\partial\tau^4$ is the Fourier transform – is narrow band, whereas that from the entire jet is a broad-band summation of these narrow bands. The autocorrelation, being a Fourier transform of this broad-band spectrum, will differ in character from $\partial^4 g/\partial\tau^4$. Thus the correspondence relating an average $\partial^4 g/\partial\tau^4$ to the experimental correlation alluded to in the last paragraph is not justified in a detailed way. Nevertheless, the final sentence of the last paragraph is still believed to provide an explanation of the negative excursions in figures 8 and 11, but in a general, rather than detailed, fashion.

Characterization of the source region as noncompact and essentially incoherent neither proves nor disproves a significant role for large-scale coherent structures in the generation process. Spatially, the reported structures are more long-scale than large-scale: they are characterized by long, convoluted vortex filaments. When included in more random turbulence, the structures do not appreciably modify measurements of instantaneous two-point correlations; such measurements in a jet indicate spatially coherent regions of only modest dimensions, for example, less than the jet diameter in the mixing region. Thus the effective average size of the coherent regions is small for sound-generation purposes.

Another interpretation is this. A large-scale coherent structure may display a certain time scale when sensed by pairs of probes of fixed separation following the mean flow, but when sensed at points each of which follows the local flow, will exhibit a stretched-out or extended time scale. It is in this time sense that the structures are especially coherent. Now although the large spatial scale (say L') of the coherent region increases its radiative efficiency, this will be more than offset by its extended time scale or reduced

characteristic frequency (say ω_f'). In fact, the mean-square pressure at a field point emitted from unit volume is proportional to $L'^3\omega_f'^4$ (e.g., ref. 17). Thus the large-scale coherent structures are not particularly effective sound generators. An exception to this statement might be made for axisymmetric structures, for example, ring vortices; however, Maestrello's measurements are incompatible with any appreciable component of axisymmetric emission in the jet noise.

CONCLUSIONS

An extensive series of measurements of two-point far-field correlations of jet noise have been carried out by Maestrello and reported in NASA TM X-72835. The results displayed some surprising features, and this motivated the present attempt at a theoretical explanation. The predictions of the theory have been compared with Maestrello's measurements, and the following conclusions are drawn:

1. Despite a number of simplifying assumptions the predictions of the theoretical model conform well with experimental results: (a) they exhibit the characteristic cusp in the curves of two-point correlation plotted against microphone separation, and (b) more than that, in most cases the quantitative curves are predicted reasonably well.

2. The analysis indicates that the shape of the curves is dominated by differences in travel times from a source to the two microphones. This is a consequence of noncompactness of the source region compared with a typical wavelength of sound. It shows up most markedly in the relative narrowness of directional lobes in the plane of the jet axis (case II) as compared with those in planes perpendicular to the jet axis (case I). These features are correctly predicted by the theory.

3. Characterization of the source region as noncompact and essentially incoherent neither proves nor disproves a role for large-scale coherent structures in the noise-generation process: the reasons are detailed in the Discussion. However, the demonstrated absence of axisymmetry in the correlation pattern rules out any significant role for axisymmetric source structures.

4. As a further corollary to conclusion 2, the basic directivity arising from the composite nature of the sources makes but a minor contribution to the correlation curves. It is, however, distinctly discernible in the curves of case I at a polar angle of 90°.

5. A variation of the "beam pattern" concept of Maestrello and Pao (J. Acoust. Soc. America, vol. 57, no. 4, Apr. 1975, pp. 959-960; NASA TN D-8104; and NASA TN D-7269) accounts for the basic directivity. The sound emission from each small volume is seen to consist of a rather directional quadrupole pattern whose lobes (and amplitude) fluctuate randomly in direction. Computation of the time average recovers the smooth patterns of basic directivity obtained herein by other methods.

6. Effects of convection of the sources and the sound waves by the flow are excluded from the theory; they are expected to cancel partially in the normalization of the correlations. There will be a residual effect resulting from altered travel time differences to the two microphones. This is estimated to be in the direction to improve the agreement with experiment; however, its inclusion would pose a formidable task.

7. The foregoing conclusions refer to the two-point correlation at zero time delay. An alternative format – with time delay reintroduced – is its Fourier transform, the cross-spectral density; this separates out the contributions of different frequencies. The differential travel time effect (cf. conclusion 2) would be expected to be relatively unimportant at low frequencies (e.g., at wavelengths equal to or greater than 2π times the jet diameter). Maestrello has recently made Fourier transforms (as yet unpublished) of his correlation measurements which indeed appear to show this. Thus, conclusions 2 and 4 do not carry over to the cross-spectral densities at the lower frequencies.

By way of closure a general observation may be made. A valid physical model of jet-noise generation must be compatible with the major features of both single-microphone intensity patterns and two-microphone correlation patterns. The model central to the present work, developed in the sixties, meets this criterion. The newer models in the literature remain to be tested.

Langley Research Center
National Aeronautics and Space Administration
Hampton, VA 23665
September 13, 1976

APPENDIX A

QUADRUPOLES WITH FLUCTUATING ORIENTATION: THE BEAM PATTERN CONCEPT

The beam pattern concept discussed in the body of the paper is most simply illustrated via the shear-noise quadrupoles. According to reference 4, equation (15), the contributing quadrupoles are

$$\begin{aligned} T_{11} &= \rho v_1^2 & T_{12} &= \rho v_1 v_2 & T_{13} &= \rho v_1 v_3 \\ &= \rho U u_1 & &= \rho U u_2 & &= \rho U u_3 \end{aligned} \tag{A1}$$

For a general quadrupole T_{ij} occupying unit volume, the contribution to far-field pressure is

$$p_{ij} \propto \frac{x_i x_j}{x^2} \frac{\partial^2 T_{ij}}{\partial t^2} = \text{Directional factor} \times \frac{\partial^2 T_{ij}}{\partial t^2} \tag{A2}$$

where

$$\left.\begin{aligned} x_1 &= x \cos\theta \\ x_2 &= x \sin\theta \cos\varphi \\ x_3 &= x \sin\theta \sin\varphi \end{aligned}\right\} \tag{A3}$$

$$\left.\begin{aligned} \frac{x_1 x_1}{x^2} &= \cos\theta \\ \frac{x_1 x_2}{x^2} &= \cos\theta \sin\theta \cos\varphi \\ \frac{x_1 x_3}{x^2} &= \cos\theta \sin\theta \sin\varphi \end{aligned}\right\} \tag{A4}$$

Thus

APPENDIX A

$$
\left.
\begin{aligned}
p_{sh} &\propto a_1(t)\cos^2\theta + a_2(t)\cos\theta \sin\theta \cos\varphi + a_3(t)\cos\theta \sin\theta \sin\varphi \\
a_1(t) &= \ddot{T}_{11} \\
a_2(t) &= \ddot{T}_{12} \\
a_3(t) &= \ddot{T}_{13}
\end{aligned}
\right\} \qquad \text{(A5)}
$$

where $\ddot{}$ indicates double time differentiation.

This may be rewritten as

$$
\left.
\begin{aligned}
p_{sh} &\propto a_1(t)\cos^2\theta + A_1(t)\cos\theta \sin\theta \cos(\varphi - \epsilon(t)) \\
\tan\epsilon(t) &= \frac{a_3(t)}{a_2(t)} \qquad\qquad A_1(t) = \sqrt{a_2^{\,2} + a_3^{\,2}}
\end{aligned}
\right\} \qquad \text{(A6)}
$$

The first term accounts for the T_{11} quadrupole: its $\cos^2\theta$ pattern merely fluctuates in amplitude. The second term accounts for the T_{12} and T_{13} quadrupoles jointly: it has the directional pattern of a T_{12} quadrupole in a reference frame rotated by a fluctuating angle $\epsilon(t)$. In effect the beam pattern of this T_{12} quadrupole is fluctuating in direction somewhat as pointed out by Pao and Maestrello (refs. 11 and 12).

Sketches of the directional polars of the two components of the instantaneous shear-noise pressure p_{sh} are given in figure 15.

The two-point correlation of far-field pressure is now formed according to this fluctuating beam pattern model. From equations (A5) with $\vec{x}^a \propto \theta_a, \varphi_a$; $\vec{x}^b \propto \theta_b, \varphi_b$; for case I $\left(\theta_a = \theta_b = \theta, \quad \varphi_a = 0\right)$:

$$
\begin{aligned}
p_{sh}\left(\vec{x}^a\right)p_{sh}\left(\vec{x}^b\right) &\propto a_1^{\,2}(t)\cos^4\theta + A_1^{\,2}(t)\cos^2\theta \sin^2\theta \cos\left(\varphi_b - \epsilon(t)\right)\cos\epsilon(t) \\
&\quad + \text{Cross-product term} \\
&\propto a_1^{\,2}(t)\cos^4\theta + \frac{1}{2}A_1^{\,2}(t)\cos^2\theta \sin^2\theta\left[\cos\varphi_b + \cos\left(\varphi_b - 2\epsilon(t)\right)\right] \\
&\quad + \text{Cross-product term}
\end{aligned} \qquad \text{(A7)}
$$

The average $\overline{p_{sh}\left(\vec{x}^a\right)p_{sh}\left(\vec{x}^b\right)} \equiv R_{sh}\left(\vec{x}^a, \vec{x}^b, 0\right)$ is required. The isotropy of the turbulence dictates that all angles ϵ are equally probable irrespective of the

amplitude A_1^2. Thus, the average over the amplitudes may be carried out first – so that $a_1^2(t) \rightarrow \overline{a_1^2}$, $A_1^2(t) \rightarrow \overline{A_1^2}$ – before carrying out the average over ϵ. The probability that ϵ lies in the range $d\epsilon$ is $d\epsilon/2\pi$, so that

$$R_{sh}\left(\vec{x}^a, \vec{x}^b, 0\right) \propto \overline{a_1^2} \cos^4\theta + \frac{1}{2}\overline{A_1^2} \cos^2\theta \sin^2\theta \cos\varphi_b$$

$$+ \frac{1}{2}\overline{A_1^2} \cos^2\theta \sin^2\theta \int_0^{2\pi} \cos\left(\varphi_b - 2\epsilon\right) \frac{d\epsilon}{2\pi}$$

$$+ \text{Integrals of cross-product terms} \qquad \text{(A8)}$$

The integrals over ϵ all vanish; also it is clear from reference 4 that $\overline{a_1^2}$ and $\overline{A_1^2}$ are equal. Hence, finally

$$R_{sh}\left(\vec{x}^a, \vec{x}^b, 0\right) \propto \cos^4\theta + \frac{1}{2}\cos^2\theta \sin^2\theta \cos\varphi_b \qquad \text{(A9)}$$

Alternatively, the correlation can be expressed in terms of the angle ψ between the vectors $\vec{x}^a$ and $\vec{x}^b$, by use of equation (D5), in the form

$$R_{sh}\left(\vec{x}^a, \vec{x}^b, 0\right) \propto \frac{\cos^4\theta + \cos^2\theta \cos\psi}{2} \qquad \text{(A10)}$$

Equations (A9) and (A10) re-cover results obtained in the body of the paper by a more conventional procedure. Thus interpretation of the source terms of jet noise as quadrupoles with fluctuating orientation – the fluctuating beam pattern concept – is given strong support.

APPENDIX B

EVALUATION OF NONCOMPACTNESS FACTORS FOR CASE I:

$$\theta_a = \theta_b = \theta, \quad \varphi_a = 0$$

The double integral in equation (30) defines the noncompactness factor for self-noise. The inner integral, to be evaluated for $\tau = 0$, is

Self-noise

$$I_{se} = \frac{1}{2\pi} \int_0^{2\pi} e^{-2\omega_f |\Delta|} \, d\gamma \tag{B1}$$

Closely related integrals must be evaluated for the case of shear noise:

Shear noise

$$I_{sh} = \frac{1}{2\pi} \int_0^{2\pi} e^{-\omega_f |\Delta|} \, d\gamma \tag{B2}$$

$$J_{sh} = \frac{1}{\pi} \int_0^{2\pi} \sin^2\left(\gamma - \frac{\varphi}{2}\right) e^{-\omega_f |\Delta|} \, d\gamma \tag{B3}$$

For the present case $\theta_a = \theta_b = \theta, \quad \varphi_a = 0$, equation (32) for Δ reduces to

$$\Delta = -\frac{R}{c_o} \sin\theta \left[\cos\gamma \left(\cos\varphi_b - 1\right) + \sin\gamma \sin\varphi_b\right]$$

$$= -\frac{2R}{c_o} \sin\theta \sin\left(\frac{\varphi_b}{2}\right) \sin\left(\gamma - \frac{\varphi_b}{2}\right) \tag{B4}$$

Put

$$\left.\begin{matrix} q_{se} \\ q_{sh} \end{matrix}\right\} = \left.\begin{matrix} 4 \\ 2 \end{matrix}\right\} \frac{\omega_f R}{c_o} \sin\theta \sin\left(\frac{\varphi_b}{2}\right) \tag{B5}$$

$$\epsilon = \gamma - \frac{\varphi_b}{2} \tag{B6}$$

APPENDIX B

Because of the $\pi/2$ periodicity of the integrand, the limits of integration can be divided by 4 as well as arbitrarily shifted in phase. The phase shift can be chosen so that Δ is always positive and the $|\ |$ can be dropped. The integrals can then, with the use of equations (B5) and (B6), be written in the more convenient forms

$$I_{se} = I(q_{se}) = \frac{2}{\pi}\int_0^{\pi/2} e^{-q_{se}\sin\epsilon}\, d\epsilon \tag{B7}$$

$$I_{sh} = I(q_{sh}) = \frac{2}{\pi}\int_0^{\pi/2} e^{-q_{sh}\sin\epsilon}\, d\epsilon \tag{B8}$$

$$J_{sh} = J(q_{sh}) = \frac{4}{\pi}\int_0^{\pi/2} \sin^2\epsilon\, e^{-q_{sh}\sin\epsilon}\, d\epsilon \tag{B9}$$

Although these are very suggestive of defining integrals for Bessel functions, the limits are different and no such reduction appears possible. The integrals are, however, very amenable to numerical evaluation.

Equation (30) requires that I_{se} (eq. (B7)) have a further integration over Y_1; there are similar requirements for I_{sh} and J_{sh}. If ω_f (to which q_{se} and q_{sh} are proportional) is taken as a constant independent of Y_1, the integral merely yields a factor of unity. For a jet, however, it would be more realistic to take $\omega_f \propto Y_1^{-1}$ (cf. ff. eq. (28)), but the price would be a more troublesome Y_1-integration. This extra complication was not considered warranted in view of the other approximations in the analysis. Instead, ω_f is written as a constant $\langle \omega_f \rangle$ in equation (B5), and $\langle \omega_f \rangle$ is called an "effective" Y_1-average.

APPENDIX C

EVALUATION OF NONCOMPACTNESS FACTORS FOR CASE II:

$$\varphi_b = \varphi_a$$

The double integral in equation (30) defines the noncompactness factor for self-noise. The difference from the case treated in appendix B is in the angle specification governing Δ. There will be no loss in generality on replacing $\varphi_b = \varphi_a$ by $\varphi_b = \varphi_a = 0$, because of the axisymmetry of the jet noise. Then equation (32) for Δ reduces to

$$c_o\Delta = Y_1\left(\cos\theta_a - \cos\theta_b\right) + R\cos\gamma\left(\sin\theta_a - \sin\theta_b\right) \tag{C1}$$

The length ℓ over which Y_1 ranges is specified as mR. If the effective noise-generating region is taken as greater than 5 diameters, then $m > 10$. Thus, for most values of θ_b and θ_a the second term is much less than the first term evaluated at $Y_1 = \ell$. This disparity breaks down as $Y_1 \to 0$, but nevertheless the contribution of the second term in equation (C1) to the integral in equation (30) will normally be minor, it is thought. The exceptions are $\theta_b \approx -\theta_a$ and θ_a and θ_b near zero or 180°. In view of the mathematical complexity attendant on retaining the second term, this term will be dropped except near $\theta_b = -\theta_a$.[2] The integral in equation (30) is then approximated as

$$I'_{se} = \frac{1}{2\pi}\int_0^{2\pi} e^{-\left(2\omega_f/c_o\right)\left|\cos\theta_b - \cos\theta_a\right|Y_1}\, d\gamma$$

$$= e^{-\left(2\omega_f/c_o\right)\left|\cos\theta_b - \cos\theta_a\right|Y_1} \tag{C2}$$

The remaining integral in equation (30) is then the integral of equation (C2) over Y_1. If ω_f is treated as a constant[3] $\langle\omega_f\rangle$, the integral is

[2]The subcase $\theta_b = -\theta_a$ of case II is precisely equivalent to subcase $\varphi_b = 180^\circ$ of case I. In this subcase only the second term of equation (C1) is nonzero, and it leads to equations (46). Equations (47) are invalid for this subcase and are to be replaced by equations (46).

[3]The more realistic assumption $\omega_f \propto Y_1^{-1}$ leads to an even simpler result. However, the specification ω_f = Constant is necessary for consistency with appendix B. (See last paragraph of appendix B for the reasons for the choice therein.)

$$\left.\begin{aligned} I'_{se} &= \frac{1 - e^{-2\delta}}{2\delta} \\ \delta &= \frac{\langle \omega_f \rangle \ell}{c_o} \left| \cos \theta_b - \cos \theta_a \right| \end{aligned}\right\} \tag{C3}$$

A similar integral arises in the case of shear noise:

$$I'_{sh} = \frac{1 - e^{-\delta}}{\delta} \tag{C4}$$

The ratios in equations (C3) and (C4) approach 0/0 as $\theta_b \rightarrow \theta_a$; however, the limit is unity. This indeterminacy causes no difficulty with numerical evaluation if the case $\theta_b = \theta_a$ is approximated by $\theta_b = \theta_a + 0.001^o$.

Equations (C3) and (C4) define the noncompactness factors arising from the integral in equation (30). For the complete reduction of equation (30) into equations (34), it is necessary to use the relation $\psi = \left| \theta_b - \theta_a \right|$ for the present case, where $\varphi_b = \varphi_a$.

APPENDIX D

REDUCTION OF THE SHEAR-NOISE INTEGRAL, EQUATION (42)

The Y_1-integration in equation (42) is approximated according to the ideas of appendix B (last paragraph) by replacing ω_f by an "effective" Y_1-average $\langle\omega_f\rangle$. Then the definition equation (44), allows the result to be rewritten more compactly as

$$R_{sh}\left(\vec{x}^a,\vec{x}^b,0\right) = \left(\overline{p_{sh}^2}\right)_{max} \frac{1}{2\pi}\int_0^{2\pi}\Big[\cos^2\theta_a \cos^2\theta_b + \cos\theta_a \cos\theta_b \sin\theta_a \sin\theta_b \sin\left(\gamma - \varphi_b\right)\sin\gamma\Big] e^{-\langle\omega_f\rangle|\Delta|}\, d\gamma \qquad (D1)$$

For case I: $\theta_a = \theta_b = \theta$, $\varphi_a = 0$,

$$R_{sh}\left(\vec{x}^a,\vec{x}^b,0\right) = \left(\overline{p_{sh}^2}\right)_{max} \frac{1}{2\pi}\int_0^{2\pi}\Big[\cos^4\theta + \cos^2\theta \sin^2\theta \sin\left(\gamma - \varphi_b\right)\sin\gamma\Big] e^{-\langle\omega_f\rangle|\Delta|}\, d\gamma \qquad (D2)$$

and

$$\Delta = \frac{2R}{c_o}\sin\theta \sin\left(\frac{\varphi_b}{2}\right)\sin\epsilon$$

$$\epsilon = \gamma - \frac{\varphi_b}{2}$$

which are equations (B4) and (B6), respectively. Upon making use of integral definitions introduced in appendix B, equation (D2) can be put in the form

$$R_{sh}\left(\vec{x}^a,\vec{x}^b,0\right) = \left(\overline{p_{sh}^2}\right)_{max}\left\{\left[\cos^4\theta + \frac{1}{2}\cos^2\theta \sin^2\theta\left(\cos\varphi_b - 1\right)\right] I\left(q_{sh}\right) + \frac{1}{2}\cos^2\theta \sin^2\theta\, J\left(q_{sh}\right)\right\} \qquad (D3)$$

where

$$q_{sh} = \frac{2\langle\omega_f\rangle R}{c_o} \sin\theta \sin\left(\frac{\varphi_b}{2}\right)$$

$$I(q_{sh}) = \frac{2}{\pi}\int_0^{\pi/2} e^{-q_{sh}\sin\epsilon}\, d\epsilon$$

$$J(q_{sh}) = \frac{4}{\pi}\int_0^{\pi/2} \sin^2\epsilon\; e^{-q_{sh}\sin\epsilon}\, d\epsilon$$

which are equations (B5), (B8), and (B9), respectively.

Recall that the angle between $\vec{x}^a$ and $\vec{x}^b$ (or between $\vec{n}^a$ and $\vec{n}^b$) was defined as ψ. Thus

$$\begin{aligned}\cos\psi &= n_1^a n_1^b + n_2^a n_2^b + n_3^a n_3^b \\ &= \cos\theta_a \cos\theta_b + \sin\theta_a \sin\theta_b(\cos\varphi_a \cos\varphi_b + \sin\varphi_a \sin\varphi_b) \\ &= \cos\theta_a \cos\theta_b + \sin\theta_a \sin\theta_b \cos(\varphi_b - \varphi_a)\end{aligned} \tag{D4}$$

For the present case $(\theta_a = \theta_b = \theta,\ \varphi_a = 0)$, equation (D4) reduces to

$$\cos\psi = \cos^2\theta + \sin^2\theta \cos\varphi_b \tag{D5}$$

Equation (D3) may be reformulated in terms of ψ as

$$\begin{aligned}R_{sh}(\vec{x}^a, \vec{x}^b, 0) = \left(\overline{p_{sh}^2}\right)_{max} \frac{1}{2}\Big\{&\left(\cos^4\theta + \cos^2\theta \cos\psi\right) I(q_{sh}) \\ &+ \cos^2\theta \sin^2\theta \left[J(q_{sh}) - I(q_{sh})\right]\Big\}\end{aligned} \tag{D6}$$

REFERENCES

1. Mani, R.: A Moving Source Problem Relevant to Jet Noise. J. Sound & Vib., vol. 25, no. 2, Nov. 22, 1972, pp. 337-347.

2. Mani, R.: The Influence of Jet Flow on Jet Noise. Part I. The Noise of Unheated Jets. J. Fluid Mech., vol. 73, pt. 4, Feb. 24, 1976, pp. 753-778.

3. Ribner, H. S.: The Generation of Sound by Turbulent Jets. Vol. 8 of Advances in Applied Mechanics, H. L. Dryden and Th. von Kármán, eds., Academic Press, Inc., 1964, pp. 103-182.

4. Ribner, H. S.: Quadrupole Correlations Governing the Pattern of Jet Noise. J. Fluid Mech., vol. 38, pt. 1, Aug. 14, 1969, pp. 1-24.

5. Nosseir, N. S. M.; and Ribner, H. S.: Tests of a Theoretical Model of Subsonic Jet Noise. Aeroacoustics: Jet Noise, Combustion and Core Engine Noise, Ira R. Schwartz, ed., American Inst. Aeronaut. & Astronaut., c.1976, pp. 3-25.

6. Ribner, H. S.: The Issue of Source Terms for Jet Noise. AIAA Paper No. 76-487, Aug. 1976.

7. Maestrello, Lucio: Two-Point Correlations of Sound Pressure in the Far Field of a Jet: Experiment. NASA TM X-72835, 1976.

8. Lighthill, M. J.: On Sound Generated Aerodynamically. I. General Theory. Proc. Roy. Soc. (London), ser. A, vol. 211, no. 1107, Mar. 20, 1952, pp. 564-587.

9. Lighthill, M. J.: On Sound Generated Aerodynamically. II. Turbulence as a Source of Sound. Proc. Roy. Soc. (London), ser. A, vol. 222, no. 1148, Feb. 23, 1954, pp. 1-32.

10. Proudman, I.: The Generation of Noise by Isotropic Turbulence. Proc. Roy. Soc. (London), ser. A, vol. 214, no. 1116, Aug. 7, 1952, pp. 119-132.

11. Maestrello, Lucio; and Pao, S. Paul: New Evidence of the Mechanisms of Noise Generation and Radiation of a Subsonic Jet. J. Acoust. Soc. America, vol. 57, no. 4, Apr. 1975, pp. 959-960.

12. Pao, S. Paul; and Maestrello, Lucio: Evidence of the Beam Pattern Concept on Subsonic Jet Noise Emission. NASA TN D-8104, 1976.

13. Maestrello, Lucio: On the Relationship Between Acoustic Energy Density Flux Near the Jet Axis and Far-Field Acoustic Intensity. NASA TN D-7269, 1973.

14. Batchelor, G. K.: The Theory of Homogeneous Turbulence. Cambridge Univ. Press, 1953.

15. Lilley, G. M.: On the Noise From Air Jets. Rep. No. 20,376, British A.R.C., Sept. 8, 1958.

16. Nayar, B. M.; Siddon, T. E.; and Chu, W. T.: Properties of the Turbulence in the Transition Region of a Round Jet. UTIA Tech. Note No. 131 (AFOSR-68-2880), Inst. Aerosp. Studies, Univ. of Toronto, Jan. 1969.

17. Ribner, H. S.: Aerodynamic Sound From Fluid Dilatations – A Theory of the Sound From Jets and Other Flows. UTIA Rep. No. 86 (AFOSR TN 3430), Inst. Aerophys., Univ. of Toronto, July 1962.

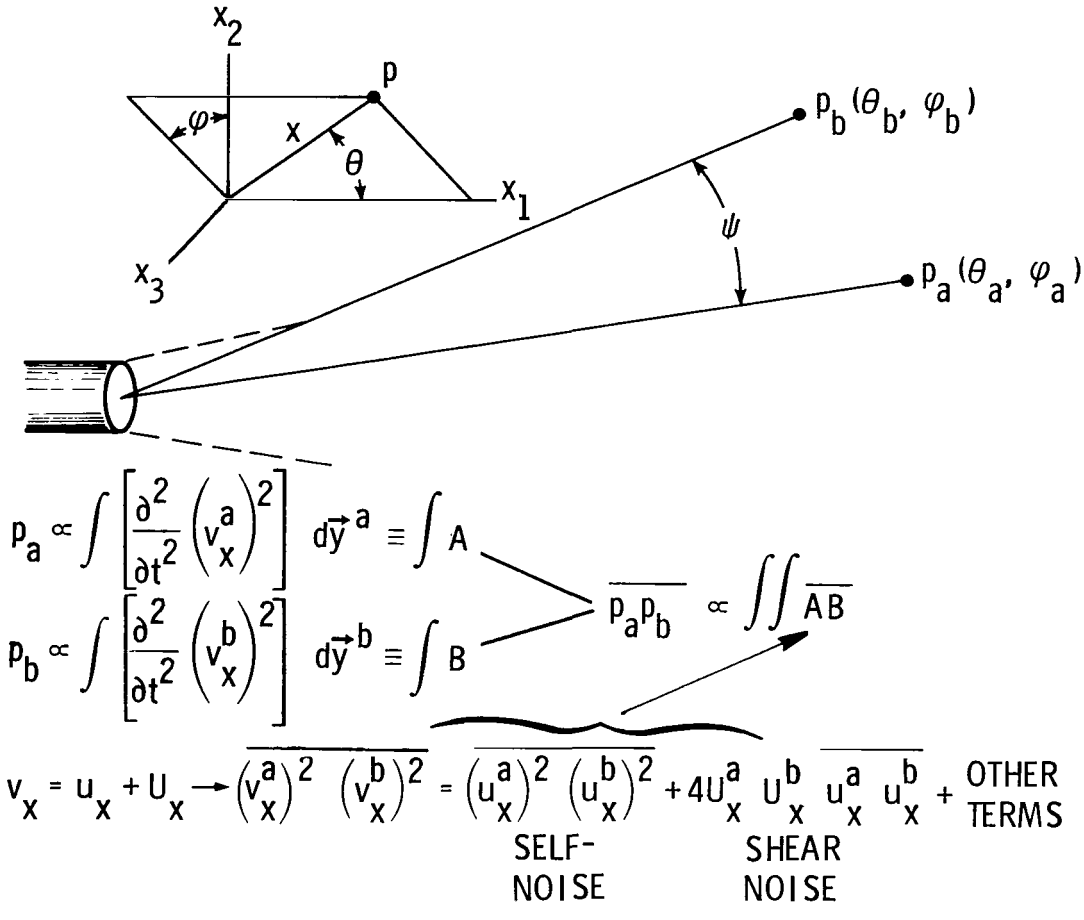

- THIS PICTURE IS GENERALIZATION OF RIBNER (1969) MODEL ($\psi = 0$) FROM $\overline{p_a^2}$ (1 MICROPHONE) TO $\overline{p_a p_b}$ (2 MICROPHONES)

Figure 1.- Scenario for deriving two-microphone correlation $\overline{p_a p_b}$.

- NEW FEATURE IS DIFFERENCE OF TRAVEL TIMES FROM SOURCE AT $\vec{Y}$ TO p_a AND p_b. THIS DIFFERENCE IS

  $\Delta = f(\psi \text{ AND OTHER ANGLES})$

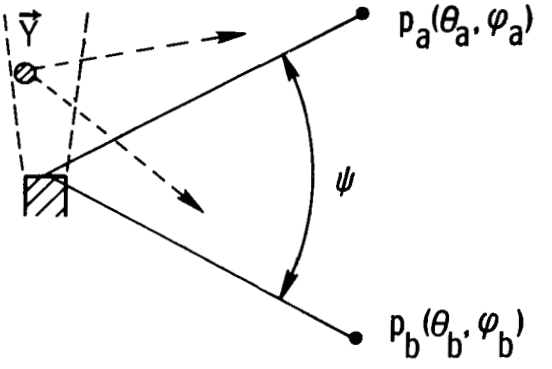

- SOURCE TERM INCLUDES

$$\frac{\partial^4}{\partial \tau^4} \overline{u_x^a u_x^b} \propto e^{-\omega_f |\tau|} \times \begin{pmatrix} \text{SPACE} \\ \text{FACTOR} \end{pmatrix}$$

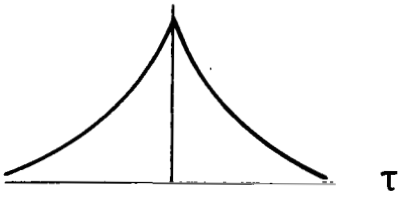

- INSERTION OF $\tau = \Delta$ YIELDS CUSP-LIKE DECAY OF $\overline{p_a p_b}$ WITH ψ AND OTHER ANGLES
- THIS IS AN EFFECT OF <u>NONCOMPACTNESS</u> OF THE SOURCE REGION

Figure 2.- Effects of difference in travel times from source to p_a and p_b (<u>noncompactness effect</u>).

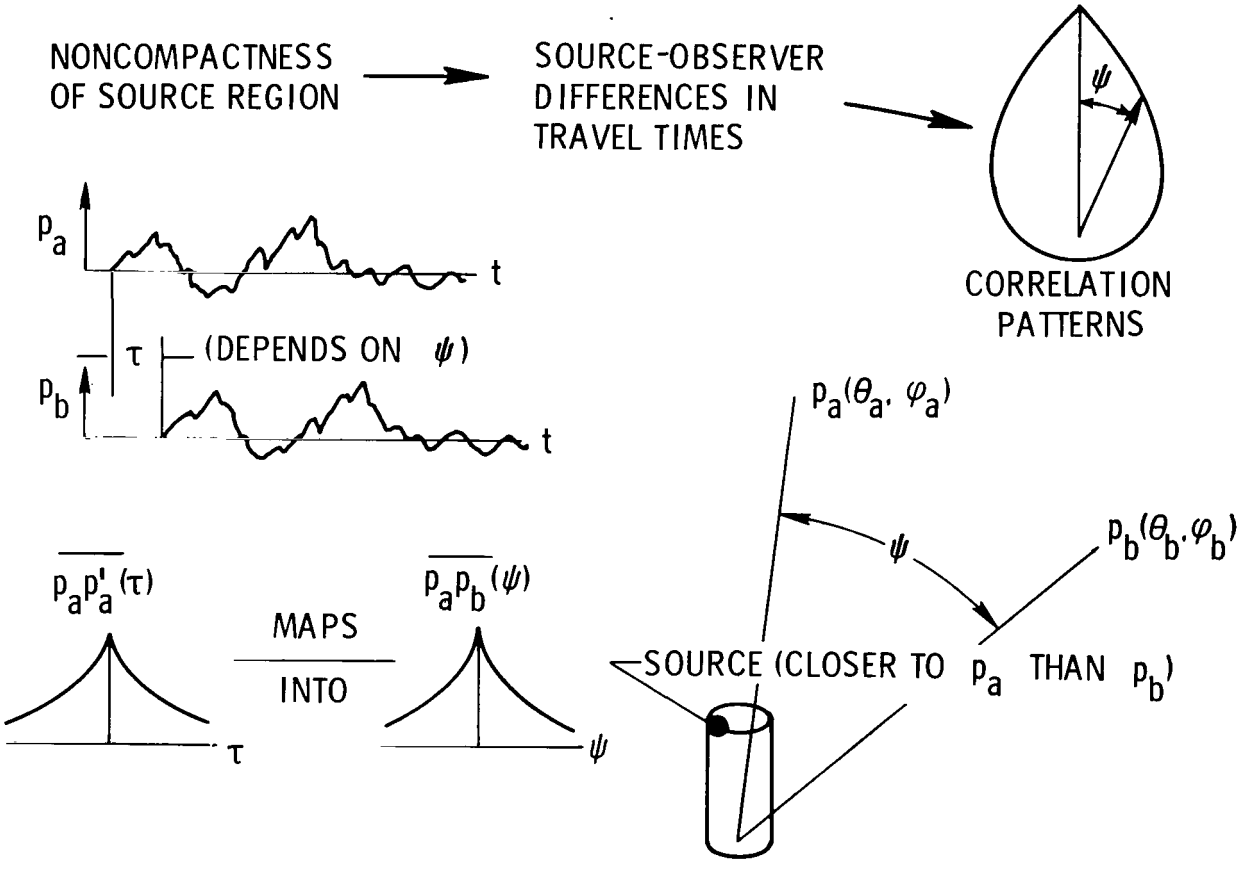

Figure 3.- Physical basis of noncompactness effect (illustrated for vertical plane).

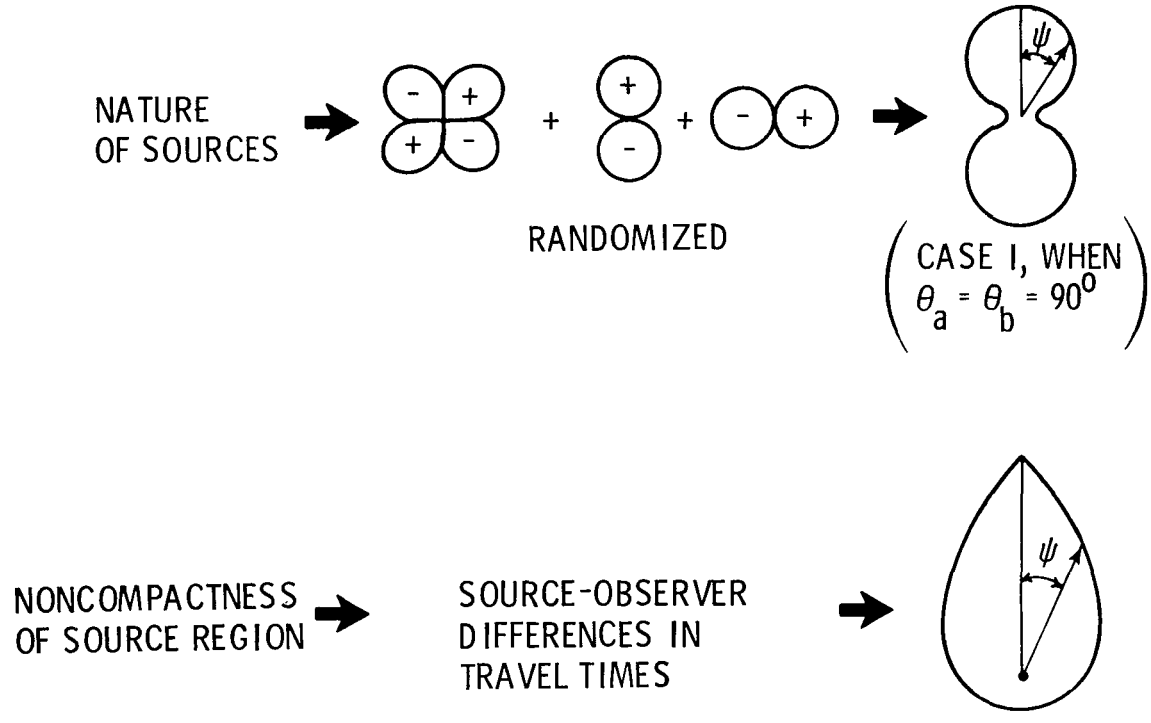

Figure 4.- $\overline{p_a p_b}(\psi) \propto$ Source directivity $\times$ Noncompactness effect.

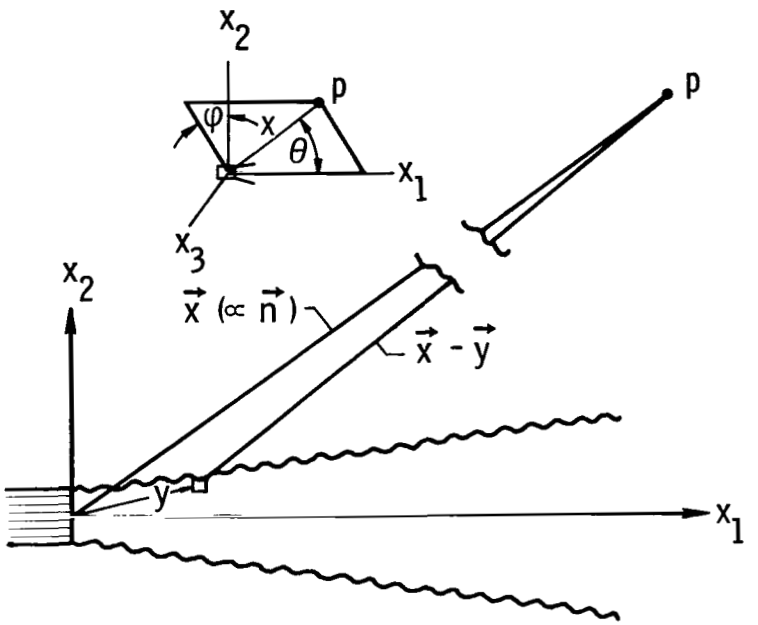

Figure 5.- Geometry of problem for one microphone.

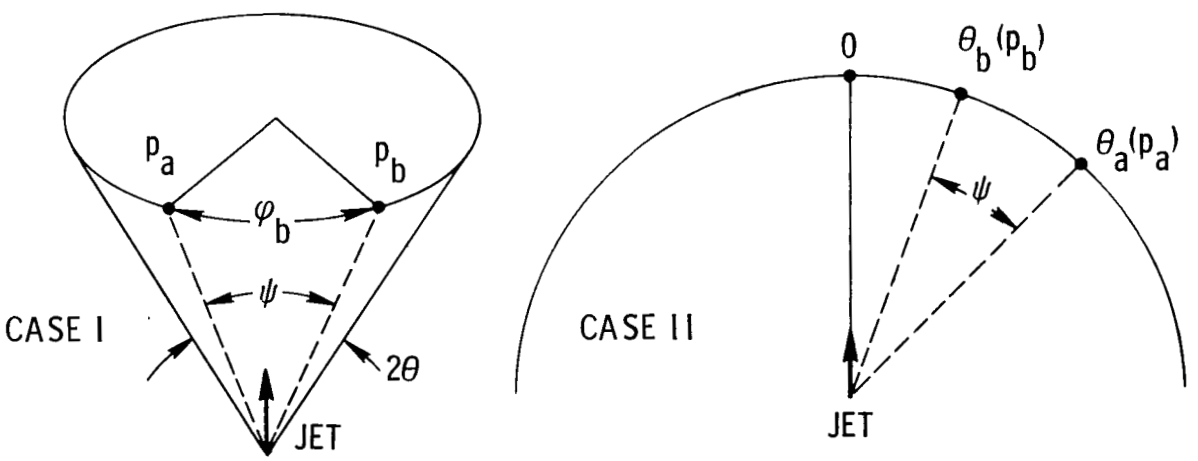

Figure 6.- Geometry of microphone positioning. Case I: Both microphones lie on a cone coaxial with jet $(\theta_a = \theta_b = \theta;\ \varphi_a = 0,\ \varphi_b$ varies$)$. Case II: Both microphones lie on a meridian circle $(\text{one at } \theta_a, \text{ one at } \theta_b)$.

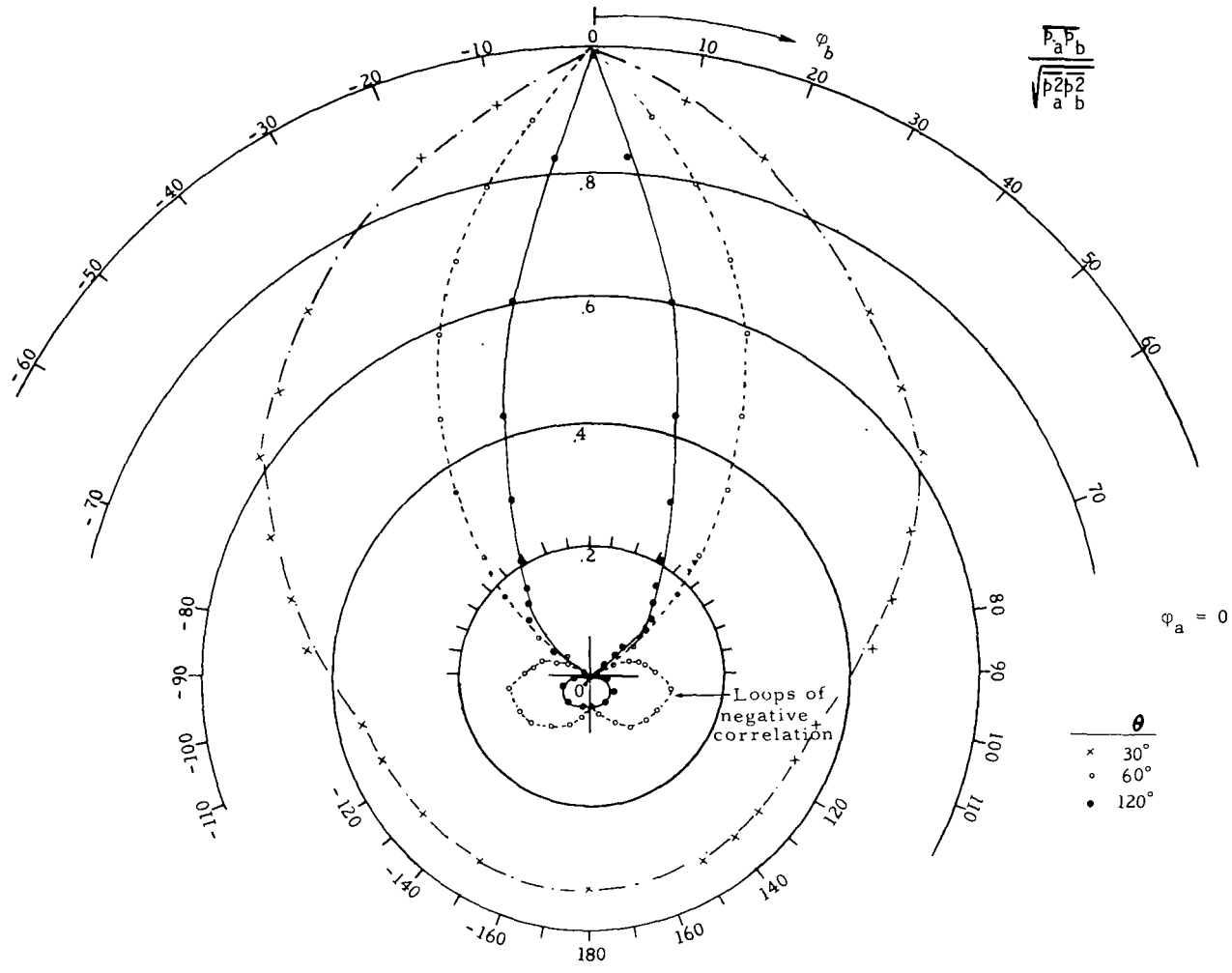

Figure 7.- Experimental polar plots of normalized $\overline{p_a p_b}(\varphi_b, \theta)$ for case I of figure 6. p_b at φ_b; p_a fixed at $\varphi_a = 0$; both on cone of half-angle $\theta = 30^o$, 60^o, and 120^o (after Maestrello, ref. 7).

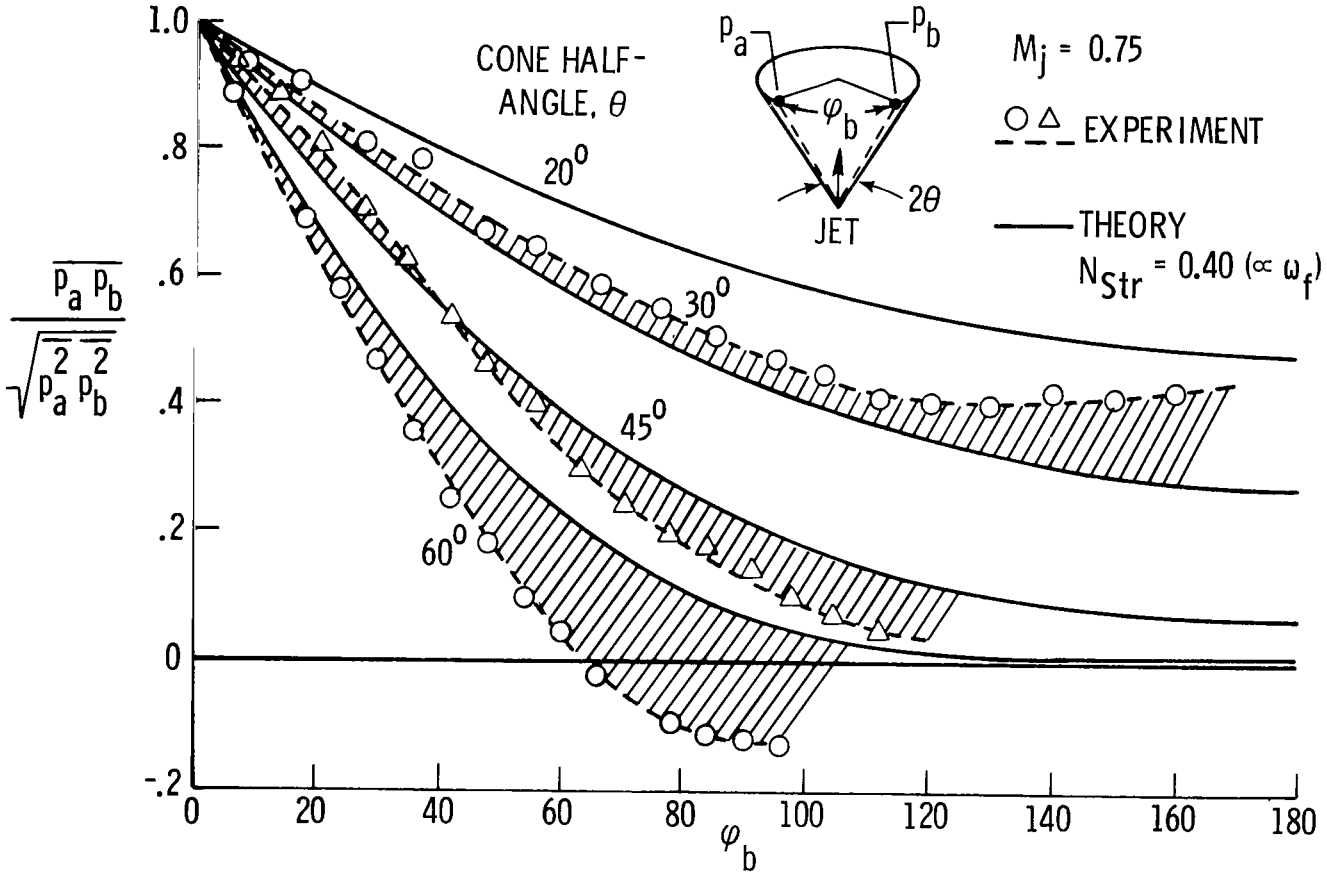

Figure 8.- Cartesian plots of normalized $\overline{p_a p_b}(\varphi_b, \theta)$ for case I of figure 6 – comparison of experiment (Maestrello, ref. 7) with present theory for $\theta = 30^o$, 45^o, and 60^o.

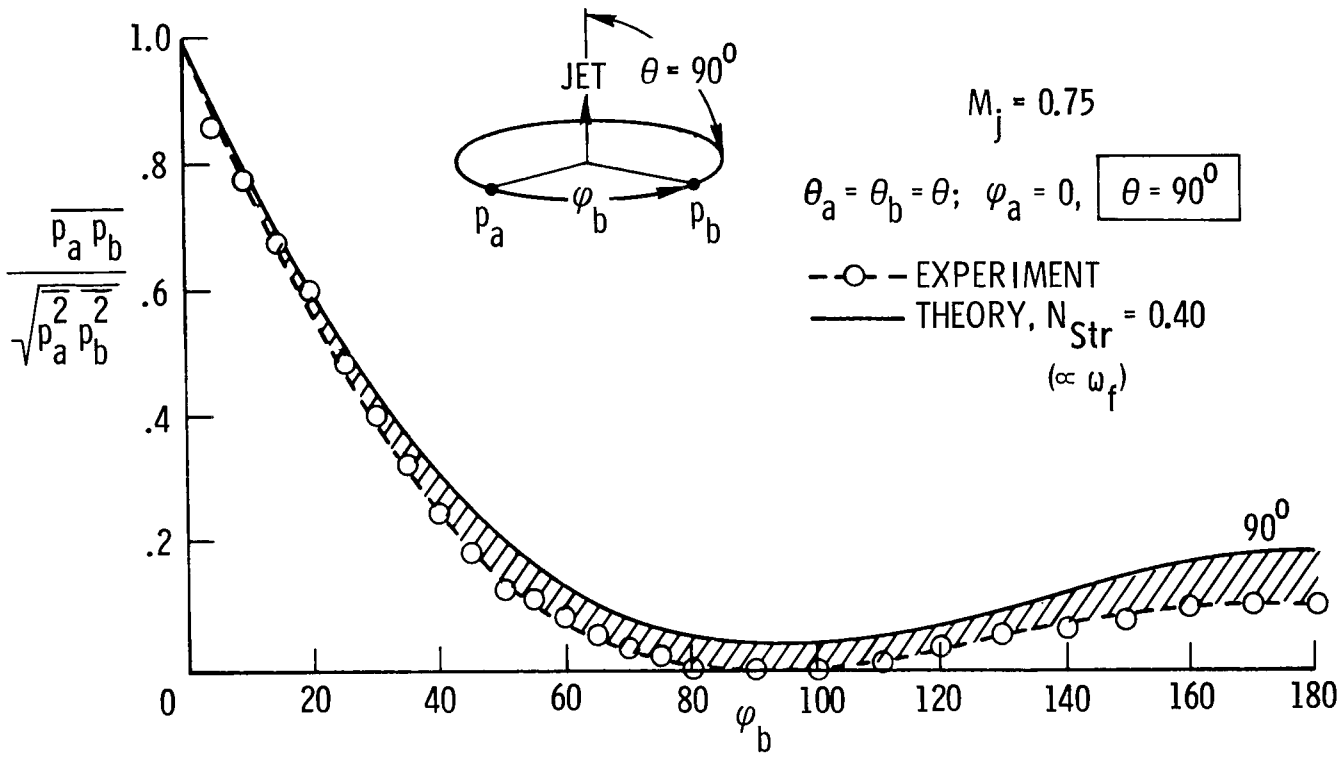

Figure 9.- Cartesian plots of normalized $\overline{p_a p_b}(\varphi_b, \theta)$ for case I of figure 6 – comparison of experiment (Maestrello, ref. 7) with present theory for $\theta = 90^0$.

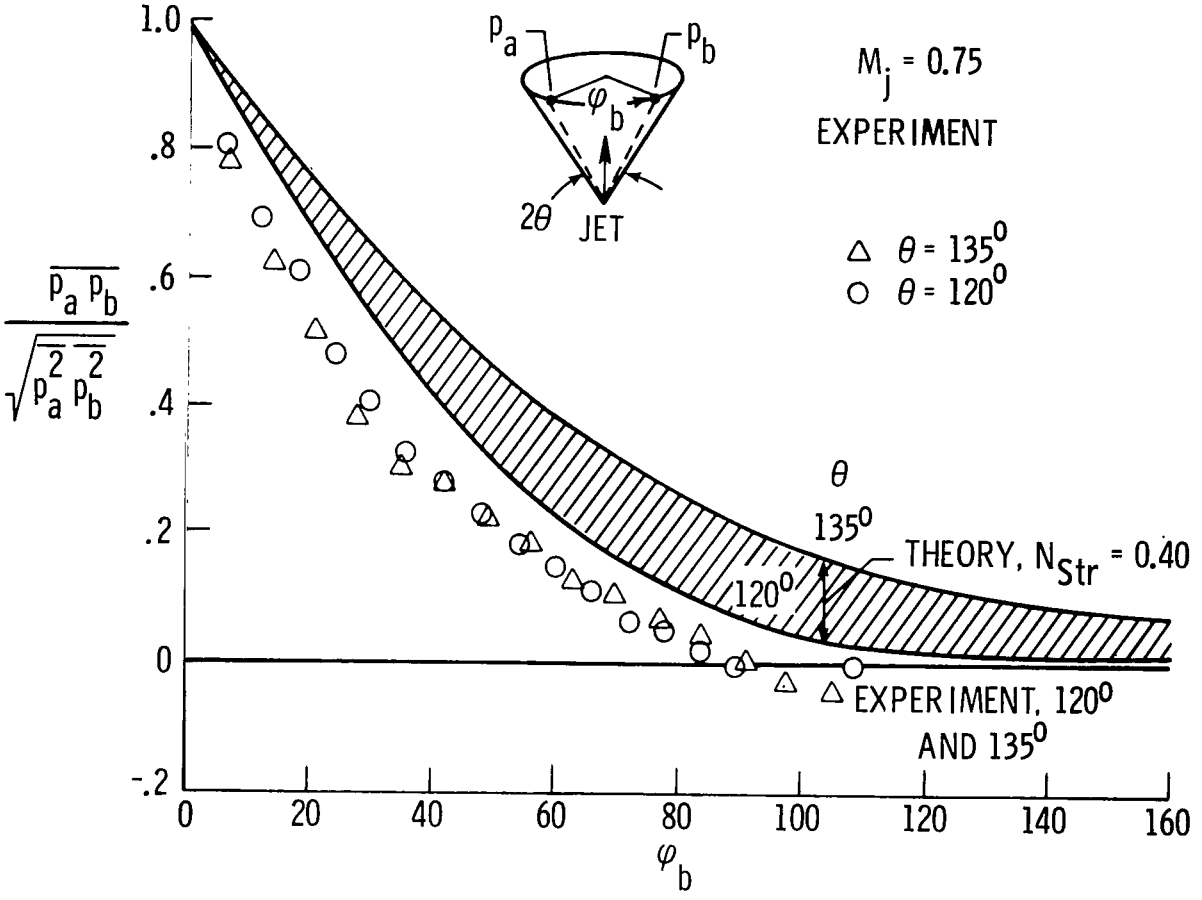

Figure 10.- Cartesian plots of normalized $\overline{p_a p_b}(\varphi_b, \theta)$ for case I of figure 6 – comparison of experiment (Maestrello, ref. 7) with present theory for $\theta = 120^0$ and 135^0.

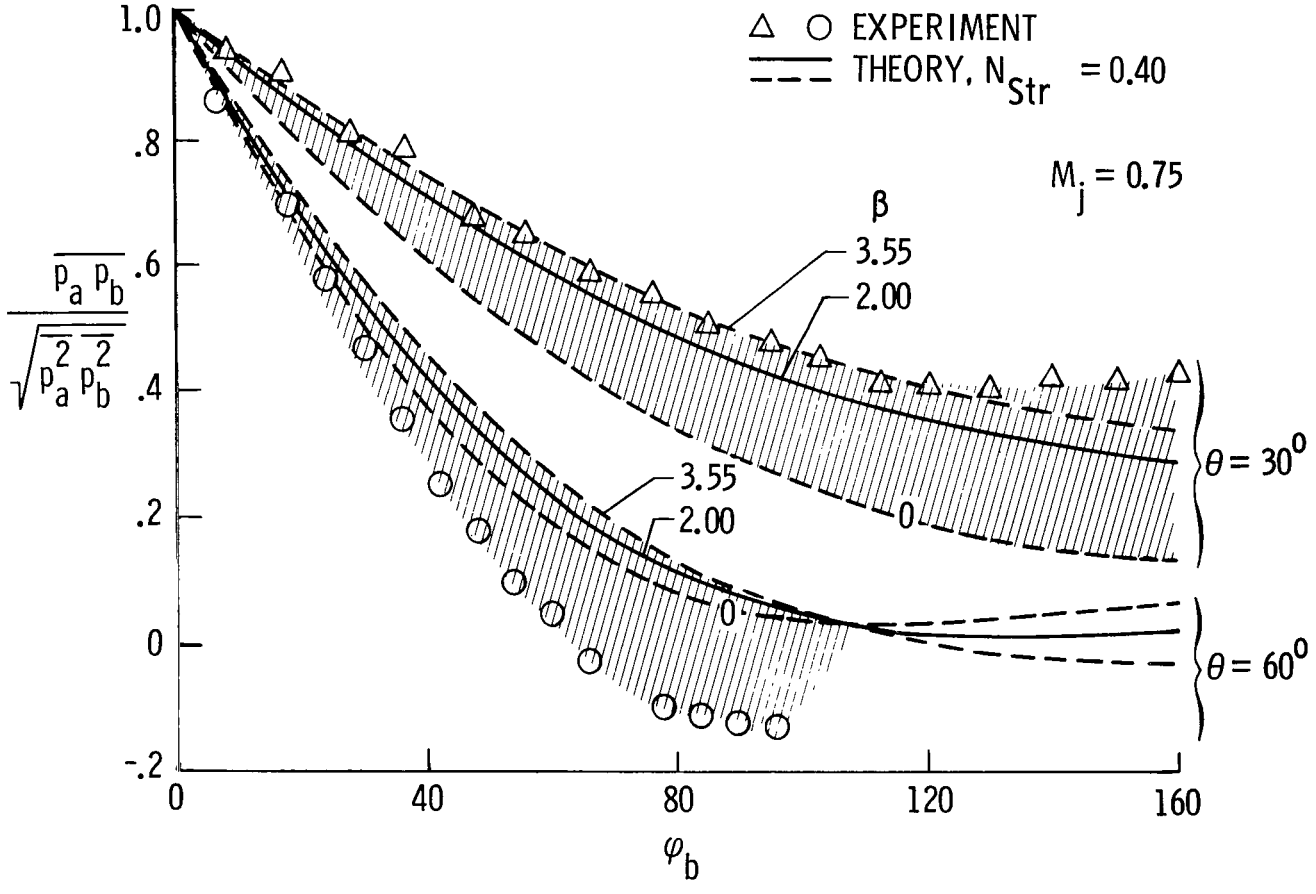

Figure 11.- Effects of shear-noise/self-noise parameter β on agreement of present theory with experiment (Maestrello, ref. 7).

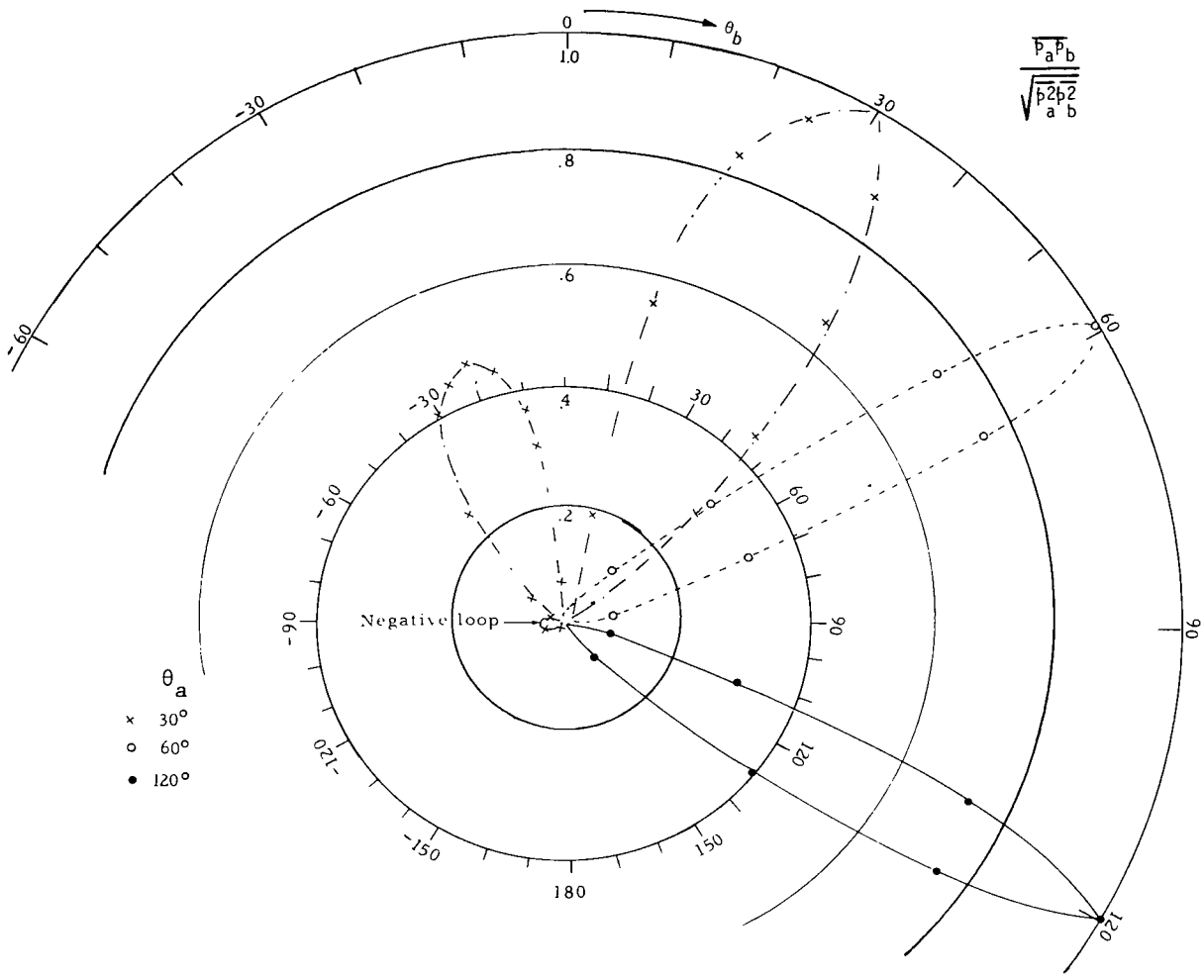

Figure 12.- Experimental polar plots of normalized $\overline{p_a p_b}(\theta_a, \theta_b)$ for case II of figure 6. p_a fixed at $\theta_a = 30^o$, 60^o, and 120^o, while angle θ_b of p_b is varied (after Maestrello, ref. 7).

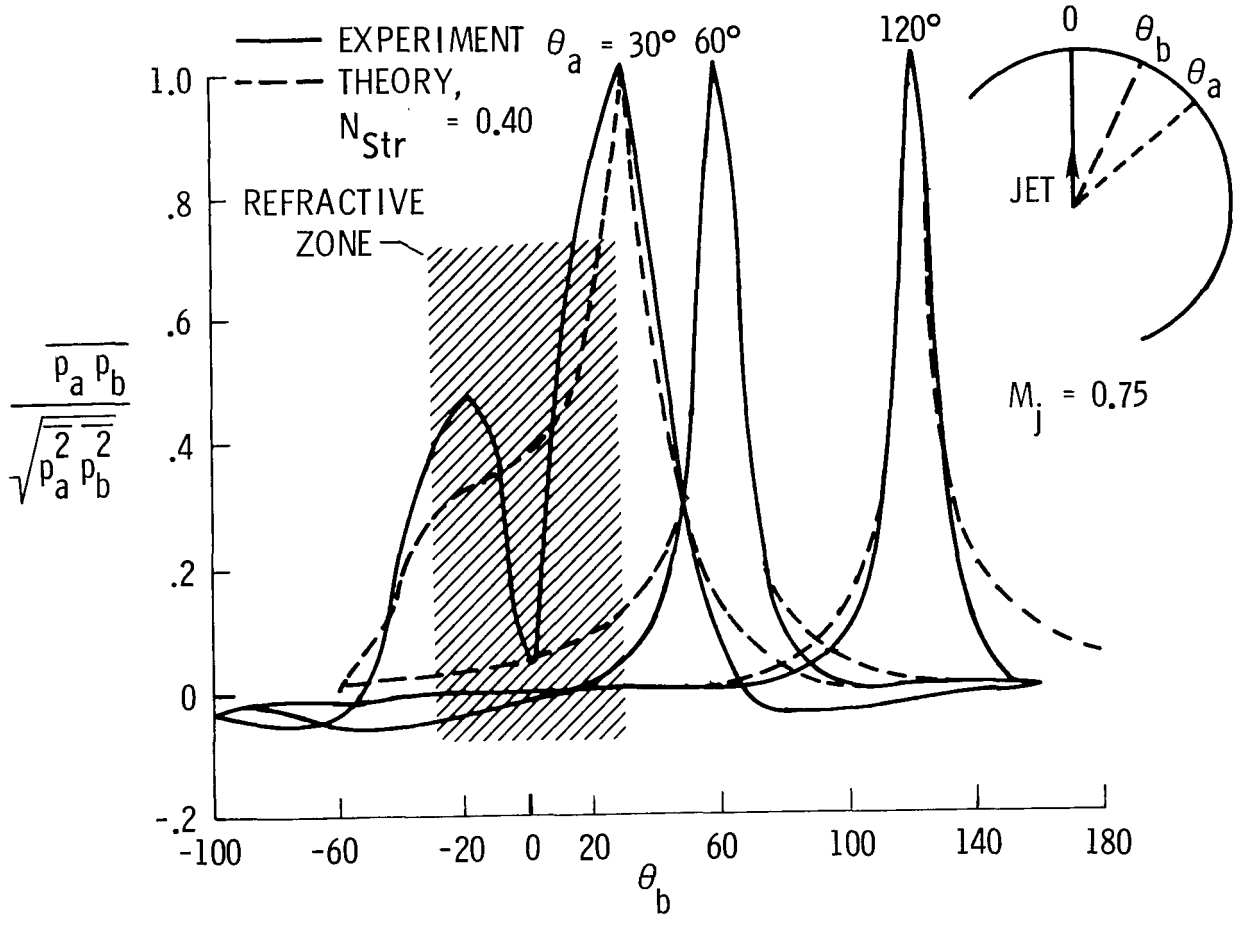

Figure 13.- Cartesian plots of normalized $\overline{p_a p_b}(\theta_a, \theta_b)$ for case II of figure 6 – comparison of experiment (Maestrello, ref. 7) with present theory for $\theta_a = 30^o$, 60^o, and 120^o.

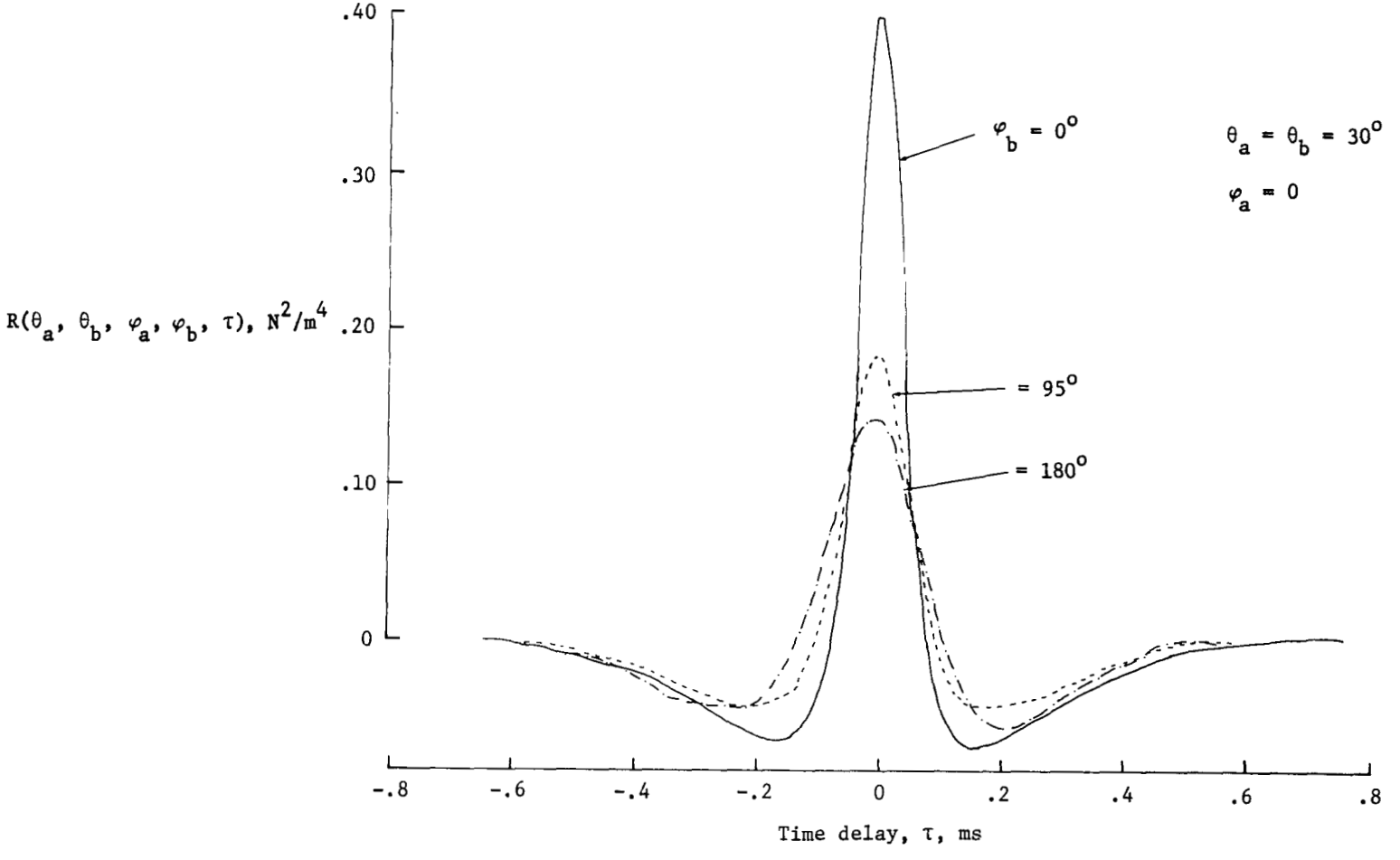

Figure 14.- Experimental cross-correlations with time delay (after Maestrello, ref. 7).

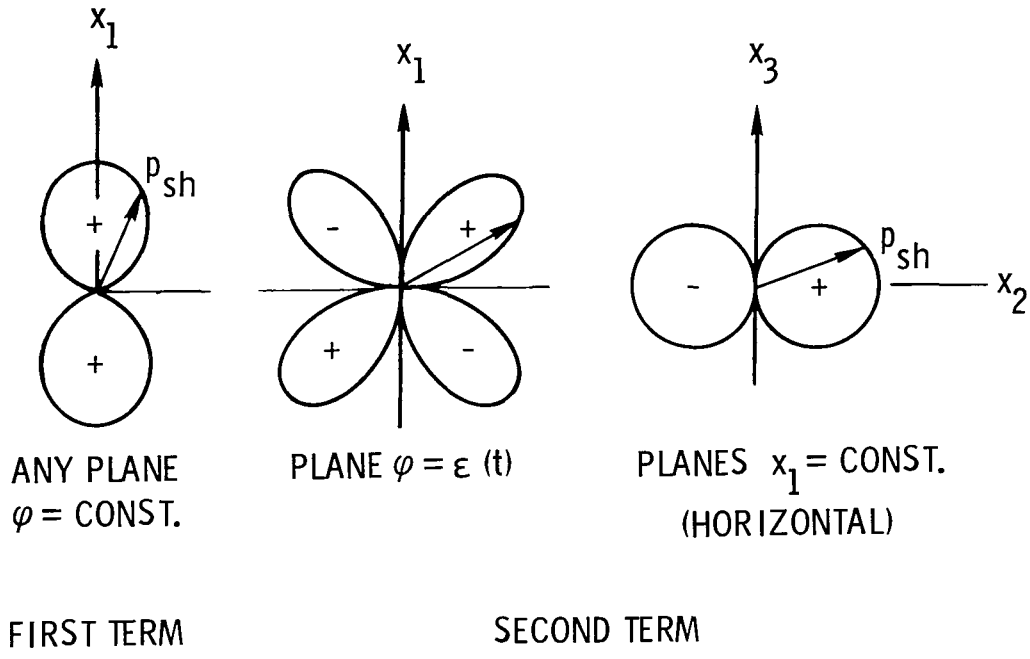

Figure 15.- Directional polars of the two components of instantaneous shear-noise pressure. The plane $\varphi = \epsilon$ fluctuates randomly in orientation (fluctuating beam pattern concept).

NASA-Langley, 1976 L-11058

"The aeronautical and space activities of the United States shall be conducted so as to contribute . . . to the expansion of human knowledge of phenomena in the atmosphere and space. The Administration shall provide for the widest practicable and appropriate dissemination of information concerning its activities and the results thereof."

—NATIONAL AERONAUTICS AND SPACE ACT OF 1958

NASA SCIENTIFIC AND TECHNICAL PUBLICATIONS

TECHNICAL REPORTS: Scientific and technical information considered important, complete, and a lasting contribution to existing knowledge.

TECHNICAL NOTES: Information less broad in scope but nevertheless of importance as a contribution to existing knowledge.

TECHNICAL MEMORANDUMS: Information receiving limited distribution because of preliminary data, security classification, or other reasons. Also includes conference proceedings with either limited or unlimited distribution.

CONTRACTOR REPORTS: Scientific and technical information generated under a NASA contract or grant and considered an important contribution to existing knowledge.

TECHNICAL TRANSLATIONS: Information published in a foreign language considered to merit NASA distribution in English.

SPECIAL PUBLICATIONS: Information derived from or of value to NASA activities. Publications include final reports of major projects, monographs, data compilations, handbooks, sourcebooks, and special bibliographies.

TECHNOLOGY UTILIZATION PUBLICATIONS: Information on technology used by NASA that may be of particular interest in commercial and other non-aerospace applications. Publications include Tech Briefs, Technology Utilization Reports and Technology Surveys.

Details on the availability of these publications may be obtained from:

SCIENTIFIC AND TECHNICAL INFORMATION OFFICE

NATIONAL AERONAUTICS AND SPACE ADMINISTRATION

Washington, D.C. 20546